

ARTICLE INFO

Editor: Pavlos Kassomenos

Keywords:

Eastern Mediterranean and Middle East region (EMME)

Pollution hotspots

In situ trace gases observations

Local vs. regional pollution

Satellite observations

ABSTRACT

Observations of key gaseous trace pollutants, namely NO, NO_y, CO, SO₂ and O₃, performed at several curb, residential, industrial, background and free-troposphere sites were analyzed to assess the temporal and spatial variability of pollution in Cyprus. Notably, the analysis utilized one of the longest datasets of 17 years of measurements (2003–2019) in the East Mediterranean and the Middle East (EMME). This region is considered a regional hotspot of ozone and aerosol pollution.

A trend analysis revealed that at several stations, a statistically significant decrease in primary pollutant concentration is recorded, most likely due to pollution control strategies. In contrast, at four stations, a statistically significant increase in ozone levels, ranging between 0.36 ppb_v y⁻¹ and 0.82 ppb_v y⁻¹, has been observed, attributed to the above strategies targeting the reduction of nitrogen oxides (NO_x) but not that of Volatile Organic Compounds (VOCs). The NO and NO_y, and CO levels at the Agia Marina regional background station were two orders of magnitude and four times lower, respectively, than the ones of the urban centers. The latter denotes that local emissions are not negligible and control a large fraction of the observed interannual and diurnal variability. Speciation analysis showed that traffic and other local emissions are the sources of urban NO and NO_y. At the same time, 46 % of SO₂ and 40 % of CO, on average, originate from long-range regional transport.

Lastly, a one-year analysis of tropospheric NO₂ vertical columns from the TROPOMI satellite instrument revealed a west-east low-to-high gradient over the island, with all major hotspots, including cities and powerplants, being visible from space. With the help of an unsupervised machine learning approach, it was found that these specific hotspots contribute overall around 10 % to the total NO₂ tropospheric columns.

1. Introduction

Air pollution is one of the most challenging problems of our era, with direct and indirect impacts on air quality, health, climate, ecosystems, economy and thus on our society. Worldwide, >4.2 M people die prematurely every year due to their exposure to outdoor pollution, according to the World Health Organization (WHO, <https://www.who.int/>). These numbers have been recently revisited by Lelieveld et al. (2019), who calculated an estimated mortality rate of 8.8 M people per year. The above figures are expected to rise further due to the ongoing urbanization.

Several studies have shown that the relationship between air quality and the economic growth of a country has an inverse “U” shape (e.g., Cole, 2003; Selden and Song, 1994). This relationship, called the Environmental Kuznets Curve (EKC), suggests that non-developed countries with minimal economic stature experience, among other environmental variables, similar air quality conditions as the most technologically advanced ones. The air quality of everybody else who lives in countries that lie between these two economic development extremes is degraded. This behavior is because economic stimulus, boosted by industrialization, is directly linked to energy consumption, which, until recently, meant the use of fossil fuels, namely coal and crude oil. WHO has set limit values to the concentrations of several emitted or secondary-produced pollutants emanating from these processes, recognizing their important role in air quality (WHO, 2005).

[Sulfur dioxide, SO₂]: As a result of the different phases of the industrial revolution, the anthropogenic component of SO₂ emitted in the atmosphere from fossil fuel combustion has constantly increased until the early 1980s (Lamarque et al., 2010). From 2002 to 2011, emission reduction in sulfur-containing compounds stimulated by strict regulations on the sulfur content of fossil fuels led to a decrease in SO₂ concentrations in the EU by approximately 33 % (Guerreiro et al., 2014). There is mixed evidence regarding the health effects of long-term exposure to elevated SO₂; some epidemiological studies suggest a direct link to mortality due to its toxicity (Burnett et al., 2004; Pope III, 2002), while others suggest otherwise (e.g., Buringh et al., 2000). SO₂ is linked to adverse effects on ecosystems as the primary factor causing acid precipitation. Regarding SO₂ climate impacts, reducing sulfate aerosol as a direct implication of reducing SO₂ has led to a global radiative forcing increase by 0.1 W m⁻² during 1990–2015 (Aas et al., 2019). This change is explained by the decreased scattering of the incoming solar radiation. During the same period over Europe, the respective change has been simulated to be 3–4 W m⁻² (Myhre et al., 2017).

[Carbon monoxide, CO]: CO, a byproduct of incomplete combustion of organic material, can be toxic and lethal in large concentrations because it hinders the ability of hemoglobin to deliver oxygen to the body. CO toxicity is associated with heart diseases and damage to the nervous system (Liu et al., 2018). Towards controlling its ambient levels, European legislation (2008/50/EU) imposes limit values on CO. Advancements in vehicular technology have decreased CO concentrations resulting in an overall 35 % decline between 2002 and 2011 in Europe (Guerreiro et al., 2014).

[Nitrogen oxides, NO_x]: Another category of regulated pollutants is the nitrogen oxides family, consisting of nitrogen monoxide and dioxide (NO_x = NO + NO₂). The dominant source of NO_x in the lower troposphere is fossil fuel combustion (Jaeglé et al., 2005; Wang et al., 2014), emitted primarily in the form of NO that is rapidly converted to NO₂ by i) O₃ or ii) organoperoxy (RO₂) and hydroperoxy (HO₂) radicals produced from the oxidation of Volatile Organic Compounds (VOCs). Short-term exposure to acute levels of NO₂ (>100 ppb) has been linked to adverse health effects (Hesterberg et al., 2009), including cardiovascular and respiratory diseases. Long-term exposure effects to lower than the above levels have also been reported (e.g., Chiusolo et al., 2011). A reduction in NO_x emissions has been reported since the mid-1980s (Lamarque et al., 2010) in the EU and USA. Despite the reported NO_x reduction of 27 % in most of the EU countries for the period 2002–2011 (European Environmental Agency, 2018; Guerreiro et al., 2014), as a result of the abatement strategies and the 2008 economic crisis (Castellanos and Boersma, 2012; Querol et al., 2014; Vrekoussis et al., 2013), the NO₂ limits set by the European Commission are frequently violated in curbside sites (Minkos et al., 2018). Notably, NO_x emissions emanating from marine traffic add significantly to the annual NO₂ mean (Viana et al., 2014). The contribution of marine traffic to NO₂ amounts has yet to be assessed for the Mediterranean Basin, the region of interest in this study.

[Ozone, O₃]: O₃ is a secondary photochemical pollutant formed in the troposphere by precursor gases such as VOC and NO_x (Seinfeld and Pandis, 2006). O₃ can also be transported from the stratosphere to the troposphere during stratospheric intrusions (Monks et al., 2015), a phenomenon that is especially strong in the Eastern Mediterranean due to the anticyclonic conditions that are frequently found during summer (Ladstätter-Weißenmayer et al., 2007; Lelieveld et al., 2009). Monsoon air is received by regions around the globe (Rauthe-Schöch et al., 2016) and was, for instance, shown to affect the tropospheric chemical composition in the Mediterranean (Lelieveld et al., 2002; Scheeren et al., 2003). Several studies have shown a linear and positive correlation between O₃ formation and temperature (Pusede et al., 2014; Weaver et al., 2009) in

the order of 1–6 ppb °C⁻¹. The linearity of this relationship has been questioned, noting that there is an upper-temperature threshold up to which this dependence is applicable (Shen et al., 2016; Steiner et al., 2010). This relation is of particular importance because, in the North Middle East region where Cyprus lies, temperatures are projected to increase faster than in the rest of the world (Zittis et al., 2016), subsequently causing O₃ concentration to elevate as well. As a result, mortality attributed to O₃ in this region is expected to increase threefold by 2050, regardless of age (Lelieveld et al., 2015). On a global scale, O₃ concentrations are significantly increased compared to the past 200 years (Forster et al., 2007; Gaudel et al., 2018; Monks et al., 2015; Volz and Kley, 1988). On average, the O₃ concentration levels from 2000 to 2012 have remained relatively steady in the EU (Guerreiro et al., 2014; Winkler et al., 2018). Similar to the rest of Europe, in Cyprus, O₃ concentrations have been reported to have a non-significant upward trend of 0.11 ± 0.12 ppb y⁻¹ recorded at a regional background site in the center of the island for the period 1997 until 2013 (Kleanthous et al., 2014).

Despite their importance, long-term studies, defined as those analyzing measurements spanning five years of data or more of gaseous pollutants in the Eastern Mediterranean and the Middle East, are scarce. Kanakidou et al. (2011) provided a comprehensive summary of pollution sources in the Eastern Mediterranean. Therein, limited long-term studies of changes in O₃ and its precursor species, namely NO₂ and CO, were reported for the urban environments of Istanbul and Athens (Kalabokas et al., 2000; Kalabokas and Repapis, 2004; Ozdemir et al., 2009) and the remote station Finokalia in Crete, Greece (Gerasopoulos et al., 2005, 2006; Kouvarakis et al., 2002). Since then, a few more long-term studies have been published concerning trace gas observations in Greece (Mavroidis and Ilija, 2012; Kopanakis et al., 2016), Nicosia (Kleanthous et al., 2014; Mouzourides et al., 2015) and Cairo (Steiner et al., 2014).

The present study investigates the short and long-term variability of gaseous pollutants in Cyprus. The island of Cyprus is geographically placed in the Eastern Mediterranean and Middle East region (EMME), an area influenced by frequent pollution events, especially during summertime (Dayan et al., 2017 and references therein). Regional background measurements of NO, NO_y, CO, SO₂ and O₃ were conducted at the regional background Agia Marina station, providing one of the longest records of those gaseous pollutants in the EMME region that is still ongoing and will be the focus

of this study; complemented by observations at the urban background and traffic stations at every major city of Cyprus. In addition, available measurements in proximity to industrial areas and a major power station will also be discussed. Further information on the monitoring stations, the instrumentation used, and the methods applied is included in Section 2. Section 3 focuses on the presentation and analysis of the temporal and spatial distribution of in situ trace gases observations in Cyprus, along with space-based observations. Section 4 provides a summary and the main conclusions of the study.

2. Methods

2.1. Monitoring stations and instrumentation

The analysis presented here is based on measurements conducted in Cyprus. The island is 250 km long and 80 km wide, covering a total area of 9250 km². The four most populated areas on the island, including suburban regions, are the inland Nicosia (capital) and the coastal Limassol, Larnaca, and Paphos cities. These four cities gather around 70 % of the island's total population (~1.2 M, Kleanthous et al., 2014). In terms of topography, Cyprus is crossed by two mountain ranges, the Troodos and Pentadaktylos Mountains (Fig. 1).

To monitor the spatial distribution of pollutants, the Department of Labour Inspection (DLI) of the Ministry of Labour, Welfare and Social Insurance led the installation and operation of a relatively dense monitoring network. Herewith, measurements from five types of stations are presented, namely *traffic-curbside* (Nicosia, Larnaca, Limassol, Paphos, Paralimni), *residential* (Nicosia, Larnaca), *industrial* (Zygi, Mari), *regional-background* (Agia Marina Xyliatou, Cavo Greco, Inia) and *free-troposphere* (Troodos) stations. The urban traffic stations operate close to the main highways and major routes in each city, at 4 m above ground (Pikridas et al., 2018). The suburban stations are placed in residential areas. The industrial stations Zygi and Mari operate close to the island's main power plant (PP1 in Fig. 1) at a distance of 4.0 and 1.3 km, respectively.

A key station for the East Mediterranean region is the regional background monitoring station at Agia Marina Xyliatou, also known as the regional background station of the Cyprus Atmospheric Observatory (CAO: <https://cao.cyi.ac.cy/>); since 1997, it provides air quality data while, in



Fig. 1. Spatial distribution of urban-traffic (red circles), residential (orange hexagons), industrial (grey squares), background (blue rhombus) and free-troposphere (white sphere) monitoring stations in Cyprus. The yellow star symbols indicated with PP_x (x = 1 to 5) labels show the location of the five powerplants of the island. The two white arrows depict the two major mountain complexes in Cyprus, namely Troodos and Pentadaktylos.

2015, it was upgraded to a superstation covering a large number of high-quality aerosol and trace-gases observations. Agia Marina Xyliatou (AGM or AMX; both abbreviations are used in the literature) serves as a member of the ACTRIS (<https://www.actris.eu/>), EMEP (<https://www.emep.int/>) and AERONET (<https://aeronet.gsfc.nasa.gov/>) networks. Geographically, AMX is located in the island's center, close to an evergreen forest at 532 m above sea level (a.s.l.). No major anthropogenic activity takes place in the vicinity of the station. Minor influences emanate from the nearby small village of Agia Marina Xyliatou, hosting 600 inhabitants at a 1 km distance.

Additional background measurements presented in this study were recorded for a period of six years (2011–2016) at the western part of Cyprus (Inia rural-marine station, 672 m a.s.l.) and at the south-eastern coastal part of the island (rural-marine Cavo Greco station, 23 m a.s.l.). The latter is closer to the ground and more exposed to the see-breeze circulation than the Inia station (Kleanthous et al., 2014). Finally, background free-tropospheric conditions met at the Troodos Mountain were captured

by a monitoring station at the top of the mountain at 1819 m a.s.l. (2013–2017).

The data archive reported in this work originates from the air quality network of Cyprus operated by the Department of Labour Inspection (<http://www.airquality.dli.mlsi.gov.cy/>). Overall, the study covers observations reported for 2003–2019 (including 2019), wherever available. Details on the span of the measurements, the reported stations' geolocation and the acronyms used are presented in Table 1.

The same table provides information on the specific instrumentation used to monitor O₃, total nitrogen oxides (NO_y), SO₂ and CO. In brief,

- O₃ was measured with UV photometric O₃ monitors (Thermo 49i at NIC_T and TRO_F and Ecotech 9810B at the rest of the sites);
- NO_y was measured with chemiluminescence monitors equipped with molybdenum converters (Thermo 42i at NIC_T and TRO_F before July 2017, replaced by Serinus 40 afterward; Ecotech 9841B or 9841T was operated during the entire period except at LIM_T, PAP_T where it was replaced by

Table 1

Information summary of the 13 monitoring sites in Cyprus presented in this study, including the location of the station and its span of operation, its acronym coordinates and altitude, along with the instrumentation used.

Station location, type, date of operation	Acronyms used	Coordinates		Altitude (m)	Instrumentation
Nicosia (Traffic-Urban) (2009–2019)	NIC _T or NIC _{TRA}	35 09'07"	33 20'52"	176	O ₃ : Thermo49i NO _y : Thermo 42i, Serinus 40 SO ₂ : Ecotech 9850, Serinus 50 CO: Ecotech 9830, Serinus 30
Nicosia (Residential) (2006–2019)	NIC _R or NIC _{RES}	35 07'37"	33 19'54"	208	O ₃ : Ecotech 9810B NO _y : Ecotech 9841 SO ₂ : Ecotech 9850, Serinus 50 CO: Ecotech 9830, Serinus 30
Larnaca (Traffic-Urban) (2003–2019)	LAR _T or LAR _{TRA}	34 54'60"	33 37'39"	15	O ₃ : Ecotech 9810B NO _y : Ecotech 9841 SO ₂ : Ecotech 9850 CO: Ecotech 9830, Serinus 30
Larnaca (Residential) (2006–2016)	LAR _R or LAR _{RES}	34 54'49"	33 36'57"	17	O ₃ : Ecotech 9810B NO _y : Ecotech 9841 SO ₂ : Ecotech 9850 CO: Ecotech 9830, Serinus 30
Limassol (Traffic-Urban) (2006–2019)	LIM _T or LIM _{TRA}	34 41'10"	33 02'08"	19	O ₃ : Ecotech 9810B NO _y : Ecotech 9841, Serinus 40 SO ₂ : Ecotech 9850 CO: Ecotech 9830
Paphos (Traffic-Urban) (2006–2019)	PAP _T or PAP _{TRA}	34 46'22"	32 25'05"	40	O ₃ : Ecotech 9810B NO _y : Ecotech 9841, Serinus 40 SO ₂ : Ecotech 9850 CO: Ecotech 9830, Serinus 30
Paralimni (Traffic-Urban) (2017–2019)	PAR _T or PAR _{TRA}	35 02'45"	33 58'40"	72	O ₃ : Ecotech 9810B NO _y : Ecotech 9841 SO ₂ : Ecotech 9850 CO: Ecotech 9830, Serinus 30
Mari (Industrial) (2011–2019)	MAR _I or MAR _{IND}	34 44'14"	33 17'24"	88	O ₃ : Ecotech 9810B NO _y : Ecotech 9841 SO ₂ : Ecotech 9850 CO: Ecotech 9830, Serinus 30
Zygi (Industrial) (2002–2019)	ZYG _I or ZYG _{IND}	34 43'46"	33 20'15"	9	O ₃ : Ecotech 9810B NO _y : Ecotech 9841 SO ₂ : Ecotech 9850 CO: Ecotech 9830, Serinus 30
Agia Marina Xyliatou/Cyprus Atmospheric Observatory (Regional background) (2003–2019; O ₃ monitoring started in 1997)	AGM _B or AGM _{BGR} or CAO	35 02'17"	33 03'28"	532	O ₃ : Ecotech 9810B NO _y : Ecotech 9841 SO ₂ : Thermo 43i-TLE CO: Ecotech 9830
Cavo Greco (Regional background) (2011–2016)	CVG _B or CVG _{BGR}	34 57'42"	34 04'54"	23	O ₃ : Ecotech 9810B NO _y : Ecotech 9841 SO ₂ : Ecotech 9850 CO: Ecotech 9830, Serinus 30
Inia (Regional background) (2011–2016)	INI _B or INI _{BGR}	34 57'44"	32 22'37"	672	O ₃ : Ecotech 9810B NO _y : Ecotech 9841 SO ₂ : Ecotech 9850 CO: Ecotech 9830, Serinus 30
Troodos (Free troposphere) (2013–2017)	TRO _F or TRO _{FTP}	34 56'36"	32 51'50"	1819	O ₃ : Thermo49i NO _y : Thermo 42i, Serinus 40 SO ₂ : Ecotech 9850 CO: Ecotech 9830, Serinus 30

Ecotech Serinus 40 in July 2019 and July 2017, respectively.

- SO₂ was measured with UV fluorescence monitors (Thermo 43i-TLE at AMX_B and Ecotech EC 9850B at all other sites, replaced by Serinus 50 in September 2018 at NIC_R and NIC_T).
- CO was measured with non-dispersive IR (NDIR) spectroscopy monitors (on most sites with Ecotech 9830B or 9830T replaced after July 2017 by Serinus 30, except for AMX_B and LIM_T where 9830B measurements are still ongoing).

Most commercially available NO_x monitors measure NO by applying the chemiluminescence technique. For NO₂ to be measured, it first has to be converted to NO. However, the molybdenum catalyst employed by all samplers in this study converts all odd nitrogen oxides (NO_y) to NO. As a result, the reported concentration corresponds to NO_y instead of NO_x. Even though this discrepancy is known, several studies report NO_x concentrations instead of NO_y, assuming that it dominates the NO_y. In this study, we report NO and NO_y concentrations, being accurate on what the reported concentrations represent. However, as the molybdenum catalyst has been widely employed in the past, this study's results are directly comparable to those found in literature, even if that is reported as NO_x.

For all the analyzers, quality checks including i) monthly zero and span checks, ii) calibration with standard transfer every three months, or weekly in case of an interchange of instrumentation, and iii) weekly change of inlet filters were performed following the EMEP reporting protocols. It should be noted that the interchange of instrumentation did not introduce step-changes or artificial trends in the presented dataset.

2.2. Air masses origin and classification

Following the detailed methodology presented in Pikridas et al. (2018), a source region analysis was performed for the island of Cyprus from 2011 to 2016, covering the period when observations of trace pollutants were available at all three regional background sites. The analysis was performed using the offline FLEXPART Lagrangian model (Pisso et al., 2019), driven by ERA-interim data (<https://www.ecmwf.int/>) available every 6 h in backward mode for 5 days. The analysis enabled the classification of incoming air masses into 7 clusters based on the potential emission sensitivity (PES) for the lowest 1 km (Seibert and Frank, 2004). These clusters are the “local” cluster linked with stagnant conditions (6 % of the total air masses influencing the island), the “marine” cluster where air masses of marine origin cross Cyprus from the western part of the island (9 %), the dust influenced “Africa” (7 %) and “Middle-East” clusters (12 %), and the northerly “Europe” (10 %), West Turkey (13 %) and East Turkey/SW Asia (44 %) associated with air masses emanating from polluted source regions.

2.3. Unsupervised machine learning for pollution plumes identification

To isolate the individual plumes from the surrounding ambient areas and calculate their contribution to the total NO₂ pollution of Cyprus for 2019, an unsupervised machine learning approach, namely self-organizing maps (SOM), was used (Kohonen, 1990). In unsupervised machine learning, the algorithm groups samples into classes that share common properties. SOMs are a well-established unsupervised machine learning approach based on competitive learning (Rumelhart and Zipser, 1986). Their main advantage is their ability to produce low-dimensional representations of higher-dimensional data (e.g., a dataset of *m* variables and *n* observations can be converted into a two-dimensional cluster map). The observations included in each cluster have more similarities than the original categorization of the dataset (e.g., based on spatial or temporal criteria). In this way, high-dimensional data can be easily visualized.

Synoptically, the SOM algorithm consists of four steps (Kohonen, 1990):

- Initialization: The weights of the clusters (neurons) are initialized with small random values.

- Competition: Observations are fed to the network. During this step, each cluster computes its own value. Based on the Euclidean distance to the current observation, the cluster closer to this observation acquires this value.
- Cooperation: Clusters close to the one that acquired the observation (i.e., their weights have similar values) adapt their weights to come closer to it. In such a way, neighborhoods of clusters are created, into which similar observations will fall. The closer a cluster is to the successful, or else dominant cluster, the bigger the adjustment of its weight will be.
- Adaptation: Each cluster creates a neighborhood or becomes a member of one, and the final structure of the SOM is created (Haykin, 1999). The method is described in detail in Kohonen (1990).

Falcieri et al. (2014) used this method to represent the Po River's plume variability in Italy. Bougoudis et al. (2016) used SOMs to study air quality in Athens. Although there are many approaches to choosing the number of clusters, the final choice is ambiguous and depends on the specific dataset. Here, four sensitivity tests were performed, with 9, 12, 16, and 20 clusters, respectively (Fig. S7). To avoid interferences from other parameters (e.g., spatial information, latitude, and longitude) in the formation of pollution patterns, only the satellite tropospheric NO₂ columns were used as inputs in the self-organizing maps.

3. Results and discussion

The presented analysis is based on hourly, daily, monthly and annual averages produced from an initial temporal resolution of 5 min. This information is used to assess the long-term, seasonal and diel variability of air pollution in Cyprus.

3.1. Long-term variability of air pollution in Cyprus

A statistical analysis based on the daily values of pollutants at all stations is performed and depicted in Fig. 2, in the form of a whisker plot. This plot aims at comparing daily averages, medians, and 1.5 interquartile ranges (1.5 × IQR) of nitrogen monoxide (NO), total nitrogen oxides minus nitrogen monoxide (NO_z = NO_y - NO), SO₂, CO and O₃, expressed in ppb_v. The interquartile range (IQR: Q₁ - 1.5IQR to Q₃ + 1.5IQR; with Q₁ being the lower quartile and Q₃ the upper quartile) excludes extreme statistical outliers.

The data are further sorted using two temporal filters. Solid boxes present all available daily measurements per station (as described in Table 1). The dashed boxes provide the same information for the period 1.1.2017–31.12.2019, as a means of comparison of the most recent levels of pollution. In several cases, the mean and the median values differ significantly. This deviation denotes that these datasets are skewed, i.e., they do not present a normal distribution but rather an asymmetrical one (e.g., Singh et al., 2001).

Fig. 2 allows for a quick first assessment of the air quality in Cyprus. Traffic - curb measurements at the three largest cities, Nicosia, Limassol and Larnaca, are associated with the highest median daily NO levels in Cyprus of 10.5, 8.7 and 8.1 ppb_v, respectively. NO values at the residential sites (NIC_R and LAR_R) and the remaining two smaller-scale cities, Paphos and Paralimni, ranged from 1.5 to 4.8 ppb_v. A similar range of NO concentrations has been reported for rural sites in Turkey (Kasparoglu et al., 2018). In contrast, the annual NO average levels at the small-scale city of Yanbu in S. Arabia were higher by a factor of 3 (15.6 ppb_v; Al-Jeelani, 2014) and in Mallorca of Balearic Islands (Spain) by a factor of 4 (~21 ppb_v; Cerro et al., 2015). The industrial sites presented median values close to 1.2 ppb_v. Notably, the regional background sites AMX, CVG, and INI presented much lower median NO amounts equal to 0.16, 0.10 and 0.12 ppb_v, respectively (see inner plots). The lowest NO median mixing ratio (0.04 ppb_v) was recorded at the Troodos free-troposphere

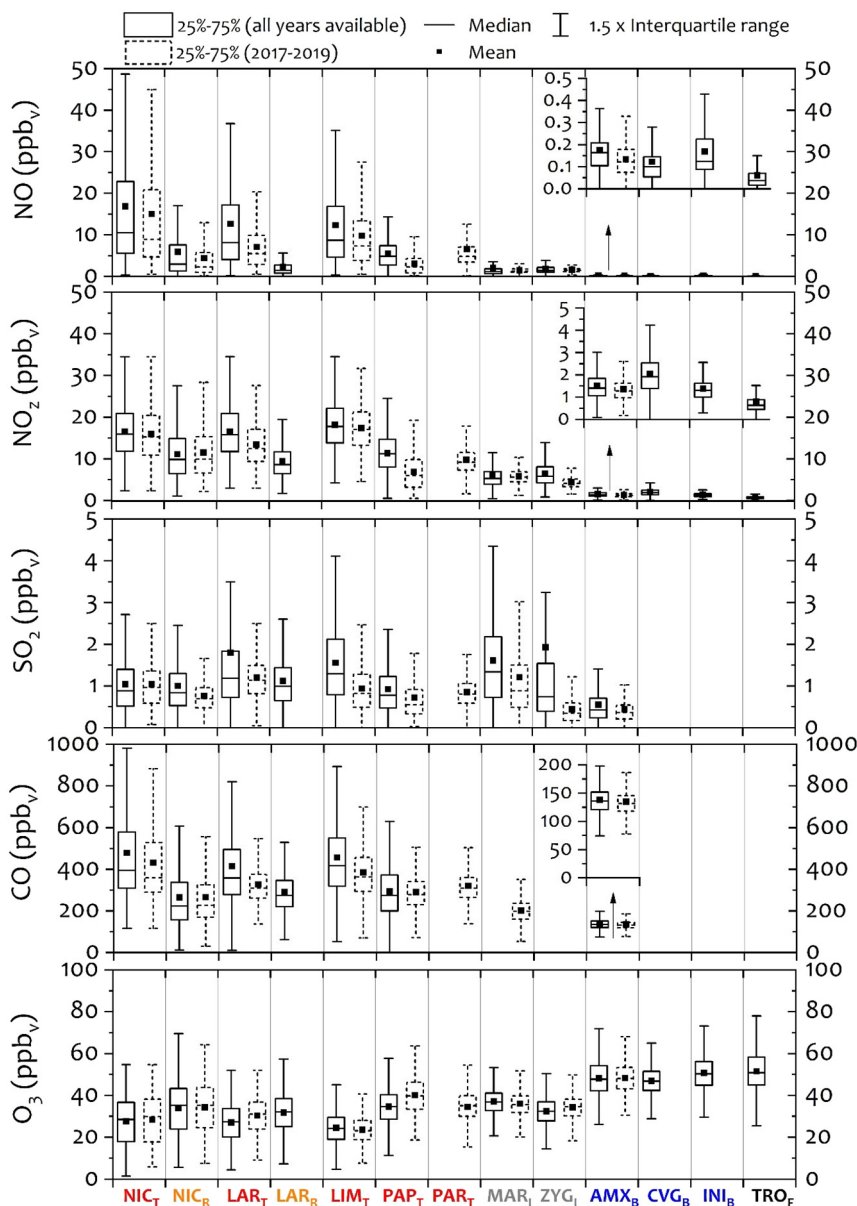


Fig. 2. Whisker plots of all available daily data (solid boxes) of trace pollutants measured at the urban-traffic (red labels), residential (orange), industrial (grey), regional background (blue) and free troposphere (black) stations. The dashed boxes provide the same information, wherever available, for the period 2017–2019. The inner plots depict the same information with a modified mixing-ratio scale range.

site. The latter is equal to the NO median reported at the Finokalia background station ~15 years ago (0.04 ppb_v; Gerasopoulos et al., 2005).

Similar results are found for the total odd nitrogen oxides and, subsequently, the NO_z. The three largest urban sites recorded the highest NO_z values (up to 17.8 ppb_v), followed by the other curb and residential sites (8.6 to 11.2 ppb_v), the industrial (5.3 and 5.8 ppb_v), the regional background (1.3 to 1.9 ppb_v) and the free-troposphere one (0.63 ppb_v). These findings are not unexpected. Nitrogen oxides have a short lifetime, typically several hours to a few days (Crutzen, 1979; Laughner and Cohen, 2019; Liu et al., 2016). Consequently, elevated amounts of these species are expected to be detected close to localized emissions such as, in the case of the curb sites, fossil fuel combustion sources associated with the transportation sector. Similar to this study, NO_x concentrations up to 18 ppb_v have been reported at an urban roadside site in Nicosia (Mouzourides et al., 2015), which lies at the lower end of the “NO_x” concentrations reported for urban areas in the Marmara region in Turkey (Kasparoglu et al., 2018), the greater Cairo area in Egypt (Khoder, 2009; Mostafa et al., 2018) and

NO₂ alone in Beirut Lebanon (Afif et al., 2009; Farah et al., 2014). The summertime regional background NO₂ levels over the Red and the Arabian Sea ranged between 1.6 and 3 ppb_v (Eger et al., 2019).

The spatial distribution of the SO₂ is different from that of NO_z. Elevated SO₂ values are encountered at the southern coastal part of the island, where three powerplants (PP1, PP2 and PP3 in Fig. 1), the biggest commercial port (Limassol) and two airports (Larnaca and Paphos) are found. For instance, at the Mari industrial station, close to PP1, the median of SO₂ was 1.3 ppb_v. In comparison, at the background station AGM, the ambient median SO₂ levels were ~3 times lower and equal to 0.4 ppb_v. An interesting point arises when comparing all available data of the period 2003–2019 and the last three years, 2017–2019. For most stations, the SO₂ has dropped significantly, mainly due to the applied mitigation strategies that have led to decreasing SO_x emissions since 2003 (EMEP center on Emission Inventories and Projections; <https://www.ceip.at/data-viewer>). A similar trend has been observed in the greater Cairo area. Over five years (2010–2014), ambient SO₂ levels decreased by half but exceeded 3 ppb_v (Mostafa et al.,

2018). Much higher concentrations of SO₂ in comparison to Cyprus have been reported for the capital of Lebanon (4.2 ppb_v; Farah et al., 2014), a small city in Saudi Arabia (6.7 ppb; Mostafa et al., 2018) and Istanbul (8.5 ppb_v; Ozdemir et al., 2009).

The reported CO medians show a similar distribution per station type as the NO_y ones pointing to emissions of common traffic sources. When compared, the highest (median) values are found for the 3 largest urban sites (359–418 ppb_v), followed by the 2 residential sites and the smaller-scale Paphos curb site (223–275 ppb_v). The lowest CO median values were recorded at the AGM (CAO) background site (136 ppb_v). Following the above overall pollution levels in the broader EMME, CO levels in Cyprus are lower than in other EMME sites. In the greater Cairo area, CO concentration has been reported to range between 3.0 and 8.3 ppm_v (Mostafa et al., 2018). In Beirut, values up to 11 ppm_v were reported (Farah et al., 2014). Notably, in the coastal small-size city of Yanbu in Saudi Arabia, the reported CO levels (165 ppb_v) are similar to those at the background site of AGM (Al-Jeelani, 2014). However, the inland Makkah city experiences much higher CO levels (1.4 to 11.3 ppm_v; Al-Jeelani, 2009), highlighting the localized contribution of fossil fuel combustion to the ambient air quality.

Lastly, the variability of O₃ showed the opposite tendency compared to the NO_z and CO. Closer to the three major urban centers of the island that are influenced by elevated localized traffic emissions, O₃ is relatively low (24.1–28.5 ppb_v) compared to its regional background levels (see text below). This behavior is mainly attributed to the titration effect when O₃ reacts with air masses rich in NO, leading to its destruction. Further away and downwind from the city centers, at the residential sites, less populated cities and industrial sites, O₃ levels are increased (32.1–36.9 ppb_v). A similar range of O₃ concentration has been reported for urban and suburban sites in Greece (Mavroidis and Ilija, 2012) and Turkey (Ozdemir et al., 2009; Kasparoglu et al., 2018). The highest medians on the island are reported for the background and free-troposphere stations (47.7–50.9 ppb_v). These values are close to those reported for the remote site of Finokalia, Greece (49–51 ppb_v; Kouvarakis et al., 2002; Gerasopoulos et al., 2005) and rural locations downwind of the megacity of Istanbul in Turkey (Kasparoglu et al., 2018) and in rural Spain (Adame and Sole, 2013). Following the pattern of an inverse correlation with NO_x levels, Beirut, Lebanon, exhibits an annual average O₃ concentration of 15.4 ppb_v (Farah et al., 2014). In Saudi Arabia, this number has been reported to be between 21.0 and 22.5 ppb_v (Al-Jeelani, 2014). Nonetheless, it should be noted that previous studies (Gerasopoulos et al., 2006; Kleanthous et al., 2014 and references therein) showed that photochemical production and destruction, although not negligible, is not the dominant mechanism associated with the presence of high O₃ levels in the region. This outcome is supported by the low local ambient levels of precursor species needed to produce O₃, such as NO_x, CO and VOCs. O₃ levels at those sites in the broader Eastern Mediterranean are controlled, to a large extent, by the synoptic meteorology bringing air masses, either a) transported from neighboring countries emitting precursor species or b) by the subsidence of air masses from the upper troposphere that is influenced by stratospheric intrusions (Kalabokas et al., 2008).

The next analysis step focuses on the multiannual variability of NO, NO_z, SO₂, CO and O₃ at all stations, depicted in Fig. S1 (Supplementary material). In this graph, each color represents one type of station to enable direct comparisons. Overall, for the primarily emitted pollutants and most station types, an apparent decreasing tendency is observed throughout the studied period. This decline is consistent with the decrease shown in the officially reported EMEP NO_x, SO_x, and CO emissions for Cyprus (Fig. S1). However, a rather increasing behavior is observed for the O₃ mixing ratios at places where anthropogenic activities occur. Similar findings have been reported in several cities globally (Adame and Sole, 2013; Cerro et al., 2015; Kumari et al., 2013). The explanation comes from the non-linear relationship of O₃ with its precursor species. Either NO_x or VOCs can limit O₃ production. In cities, where typically the VOC-to-NO_x ratio is low (VOC limited regime), a decrease in NO_x, without accounting for VOC emissions reductions will eventually lead to an increase in O₃

(Chang et al., 2016). Therefore, when planning efficient pollution control strategies, it is necessary to consider both categories of species in a manner that will lead to effective O₃ control.

To assess the magnitude and significance of the above tendencies, the same annual dataset was subjected to a statistical non-parametric Mann-Kendall trend analysis (Gilbert, 1987). The results are presented in Table 2. The analysis was conducted for the stations with ten or more years of available data. In 4 out of the 8 monitoring stations, namely in LAR_{TRA}, LAR_{RES}, PAP_{TRA}, and ZYG_{IND}, a statistically significant increase in the O₃ levels of +0.51 ppb_v y⁻¹, +0.82 ppb_v y⁻¹, +0.65 ppb_v y⁻¹, and +0.36 ppb_v y⁻¹, respectively, has been observed. These increasing trends corroborate the above findings presented in Fig. S1 and highlight the need to take measures to alleviate the magnitude of the increase. A similar increasing trend of ~ +0.7 ppb_v y⁻¹ was found in a rural area in the north-east of the Iberian Peninsula (Adame and Sole, 2013).

Statistically significant decreasing trends for NO (between -0.01 ppb_v y⁻¹ and -0.91 ppb_v y⁻¹) and NO_z (-0.06 to -0.71 ppb_v y⁻¹) were found at almost all stations in Cyprus. Comparable NO and NO₂ trends were reported for the Western Mediterranean (Cuevas et al., 2014; Cerro et al., 2015). The Mann-Kendall analysis revealed statistically significant declining slopes also for CO and SO₂ at 5 monitoring stations ranging between -1.26 to -19.80 and -0.02 to -0.27 ppb_v y⁻¹, respectively.

One point of interest is the decreasing primary pollutants trends observed at the AGM background station. This station, as mentioned, is placed far away from local emission sources. Yet, the NO, NO_z, SO₂ and CO trends show a statistically significant decline. This outcome could be attributed to pollution reduction strategies in neighboring countries influencing Cyprus and/or changes in meteorological conditions.

3.2. Seasonal variability of air pollution in Cyprus

The next step is the investigation of the seasonal variability of pollutants in Cyprus. This analysis is based on the monthly mean values of trace gases for the stations where the most recent available data (2017–2019) reflect current air quality conditions. The results, presented in Fig. 3, are summarized below.

The seasonal variability of the NO mixing ratio in all cities presents a characteristic uni-modal “U”-shape. The highest values are observed in winter and the lowest in summer. The amplitude of the high-to-low variability differs per monitoring station, with the highest value found for the Nicosia curb site (28 ppb_v). Negligible amplitude changes are found for the industrial Zygi and Mari sites and the AGM station.

The observed unimodal shape in cities is caused by changes in i) meteorology, ii) emission strengths and iii) chemistry.

i) *Meteorology*: Towards summer, the planetary boundary layer (PBL) expands, which, in turn, enables the dilution of the polluted air masses.

ii) *Emissions*: The NO emanates largely from the combustion of fossil fuels used for transportation and domestic heating. In the summertime, domestic heating emissions are negligible.

iii) *Chemistry*: Lastly, during summer, O₃ levels are higher than in winter due to enhanced insolation. As a result, more NO is oxidized to NO₂. However, here the interplay is more complex due to chemical non-linearities in the presence of VOC and the simultaneous NO₂ photolysis under high insolation.

Similarly, a marked annual cycle was observed in the case of NO_z. In all cities and the residential site, the same unimodal distribution as before is observed originating from the common sources of NO and NO_y. That is supported by nitrogen oxides closure studies (e.g., Ninneman et al., 2021), stating that in urban environments, the largest fraction of NO_z is found in the form of NO_x (NO and NO₂). At the industrial monitoring stations, and especially at the Mari station closer to PP1, a slight enhancement is observed in the NO_z levels of summer. It is hypothesized that this small enhancement is caused by the excess in power production due to the higher demand for electricity in summer (Panayiotou et al., 2010) needed to support air-conditioning usage on the island. Finally, the remote background station AGM shows practically negligible NO_z variability compared to the other

Table 2

Mann Kendall trend analysis results for the Nicosia (curb and residential), Larnaca (curb and residential), Limassol (curb), Paphos (curb), Zygi (industry) and Agia Marina (CAO, background) stations. The green color denotes a significant decreasing trend, and the yellow an increasing one. All annual changes are expressed in ppb, y^{-1} .

Monitoring Station, Period [years]	Trace gas	Slope (Q) [ppb, y^{-1}]	Level of significance
NIC TRA, All gases: 2009-2019	NO	-0.32±0.17	NS
	NO ₂	-0.12±0.09	NS
	SO ₂	-0.05±0.03	NS
	CO	-13.80±2.16	**
	O ₃	0.12±0.12	NS
NIC RES, All gases: 2006-2019	NO	-0.36±0.05	***
	NO ₂	-0.17±0.10	+
	SO ₂	-0.03±0.02	**
	CO	1.13±0.86	NS
	O ₃	-0.04±0.08	NS
LAR TRA, All gases: 2003-2019	NO	-0.91±0.28	***
	NO ₂	-0.50±0.08	***
	SO ₂	-0.09±0.12	**
	CO	-15.76±5.33	***
	O ₃	0.51±0.08	***
LAR RES, All gases: 2007-2016	NO	-0.08±0.03	*
	NO ₂	-0.20±0.08	NS
	SO ₂	0.02±0.02	NS
	CO	-11.59±6.49	+
	O ₃	0.82±0.21	**
LIM TRA, All gases: 2006-2019	NO	-0.83±0.12	***
	NO ₂	-0.48±0.08	**
	SO ₂	-0.12±0.02	**
	CO	-19.80±3.82	**
	O ₃	-0.03±0.09	NS
PAP TRA, NO, NO ₂ , SO ₂ , O ₃ : 2006-2019 CO: 2016-2019	NO	-0.50±0.05	***
	NO ₂	-0.71±0.08	***
	SO ₂	0.04±0.02	NS
	CO	<10 years	-
	O ₃	0.65±0.14	***
ZYG IND, NO, NO ₂ , SO ₂ , O ₃ : 2003-2019 CO: Not available	NO	-0.09±0.01	**
	NO ₂	-0.34±0.04	***
	SO ₂	-0.27±0.03	***
	CO	-	-
	O ₃	0.36±0.09	**
AGM BKG, NO, NO ₂ , SO ₂ , O ₃ : 2003-2019 CO: 2010-2019	NO	-0.01±0.00 ₄	**
	NO ₂	-0.06±0.02	**
	SO ₂	-0.02±0.01	**
	CO	-1.26±0.59	+
	O ₃	-0.02±0.06	NS
CVG BGR, INI BGR, TRO FTP	Data < 10 years		

*** $p < 0.001$, ** $p < 0.01$, * $p < 0.05$, + $p < 0.1$, NS $p \geq 0.1$.

stations. However, using a different mixing ratio scale (inner panel of Fig. 3), it is evident that a city-like unimodal NO₂ seasonal distribution is found, with an amplitude of 1 ppb. Because the station is far from local sources, this variability is likely attributed to regionally transported air masses.

One should also consider that contrary to cities, the NO_y budget at remote and free-troposphere places is also significantly influenced by the presence of peroxyacetyl-nitrate (PAN) (Zellweger et al., 2003). During cold conditions, PAN can be transported over long distances acting as a reservoir of NO₂, but without being decomposed to NO₂. As a result, during the winter, a significant fraction of the AGM NO_y variability could be explained by the presence of PAN. Unfortunately, no PAN measurements

were conducted in Cyprus to account for the latter. The observed annual U-shape NO₂ variability in Cyprus with maxima during winter and minima during summer has been observed in other urban cities in the EMMER region, including Lebanon and Turkey (Farah et al., 2014; Kasparoglu et al., 2018;) and elsewhere in more polluted environments (Meng et al., 2009).

The SO₂ seasonal variability is, overall, similar at all stations except for Mari. At the industrial Mari station, the highest SO₂ values are found for the warmer period in Cyprus, supporting what was hypothesized earlier based on the increased power production (Panayiotou et al., 2010). A summer SO₂ maximum is also observed at a regional background site in the Balearic Islands (Cerro et al., 2020) for similar reasons. At all other stations, the

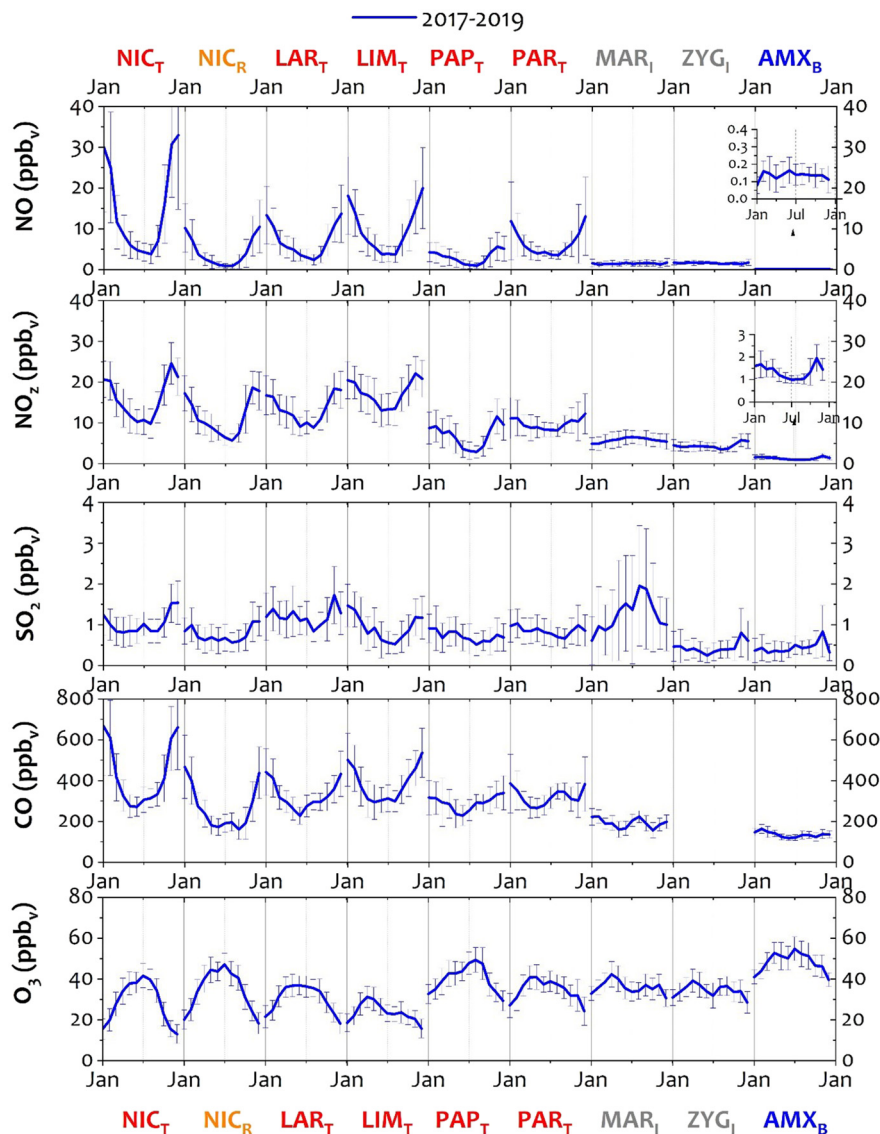


Fig. 3. Seasonal variability of trace pollutants (NO, NO₂, SO₂, CO and O₃) for the period 2017–2019 at five urban-traffic, one residential, two industrial and one regional background stations in Cyprus. The blue lines depict monthly averages coupled to their respective standard deviation.

observed variability is characterized by winter-to-summer, high-to-low SO₂ values. This variability could be attributed to emissions emanating from domestic heating and smaller-scale industrial activities and/or meteorological influences. Since the overall pattern is different from the one observed in Mari, local “contamination” from the powerplants in the southern part of the island should be disregarded. Similarities in the temporal features of the SO₂ variability, such as the peaks in June and November, suggest that regional transport contributes to the observed levels of SO₂ on the island. This conclusion is consistent with the findings reported by Afif et al. (2008) regarding Beirut, Lebanon, which is mostly downwind of Cyprus. In that work, a similar high-to-low pattern from winter to summer was observed in urban Beirut. It was estimated that approximately half of the measured SO₂ concentration (≈ 1.5 ppbv) was due to long-range transport.

Interestingly, despite having different lifetimes, the variability of CO and NO show strong similarities. In cities and residential places, CO amounts are high during winter and low during summer. CO is mainly emitted during the incomplete combustion of carbon-containing fuels. The marked seasonality can be explained, as was the case for the NO trace gas, by changes in meteorology and emissions strength. One difference evident in all stations' seasonal variability is a small secondary peak observed

in summer. This enhancement could be caused by two factors: a) the transport of air masses rich in CO during the prevailing northerlies (see Pikridas et al., 2018) and b) the higher insolation that favors the photochemical oxidation of hydrocarbons (Debevec et al., 2017, 2018) that break down to form CO and ultimately, CO₂. Strong similarities between the seasonality of NO and CO have been reported before in the EMME region (Kalabokas et al., 2000; Al-Jeelani, 2014). In these studies, CO maximized during winter, having a smaller peak during summer.

The seasonal O₃ variability is mostly unimodal but opposite to the one explained for NO, NO₂, SO₂ and CO, with the highest O₃ amounts encountered in summer. O₃ is a secondary species produced photochemically when precursor species, such as NO_x, CO and VOC, react in the presence of sunlight. Since the highest insolation occurs in summer, O₃ production should also maximize in summer. This pattern is depicted in Fig. 3, where for most of the stations, the highest O₃ is found in summer. Notably, the highest monthly O₃ means are recorded for the AGM (CAO) background station reaching 55 ppbv, in July. However, the low abundance of the NO₂ levels (1 ppbv) and CO (0.13 ppbv) in July at the AGM station, as well as the small amplitude in their annual variability, suggest that the observed ambient O₃ levels are photochemically produced regionally rather than

locally and/or regionally transported by advection and convection towards AGM due to the prevailing meteorological conditions. This is further supported by previous studies focusing on the processes controlling ozone levels in the Eastern Mediterranean region (Gerasopoulos et al., 2006; Ladstätter-Weißmayer et al., 2007; Kleanthous et al., 2014). For example, by using satellite data of O₃, NO₂ and HCHO together with box and Lagrangian model simulations, Ladstätter-Weißmayer et al. (2007) concluded that the main mechanism driving ozone in the area is long-range transport followed by regional photochemical build-up of O₃.

An exception to the above summer maximum is observed at three stations. In the curb Limassol site, O₃ is decreasing in summer. Since any regional changes would have been observed at all stations, this behavior is assumed to be caused by localized emissions leading to O₃ destruction. The local NO₂ levels in Limassol in summer are the highest among all stations and equal to around 15 ppb_v. Therefore, it is quite likely that the photolysis of the excess NO₂ produces NO that reacts with O₃ leading to its destruction.

The other two summer minima cases are observed at the industrial Mari and Zygi coastal sites. However, at both sites, the NO and NO₂ do not present significant seasonal changes, contrary to the behavior of SO₂. As mentioned before, during summer, enhanced amounts of SO₂ are observed close to PP1. We hypothesize that the uptake of O₃ favors acid displacement reactions onto sea salt aerosols present in the ambient air of the coastal areas on the island. As a result, the sulfuric acid (H₂SO₄) could be partitioned to sulfite (SO₃²⁻) and then to sulfate (SO₄²⁻) (Von Glasow, 2008). At the same time, chlorine radicals (Cl•) could be released into the gas phase. If no strong NO₂ sources are present to form ClNO₂, as is the case for the two industrial stations, the Cl• may lead to O₃ destruction and subsequent formation of ClO (Wang et al., 2019).

3.3. Weekly cycles impacting air pollution in Cyprus

The next step involved the calculation of the most recent (2017–2019) available weekly cycles based on the daily means of air pollutants. As depicted in Fig. S2, data were clustered into three categories; weekdays, Saturdays and Sundays. For all monitoring sites and types, reductions in NO are observed when shifting from weekdays to weekends.

Consistent reductions in all cities, varying by 34–51 %, are found for NO. The highest absolute decrease is found for Nicosia, where NO drops, on average, by 7.16 ppb_v, during Sunday. Lower percentages (20–34 %) and magnitudes are reported for the industrial sites (0.33–0.54 ppb_v). Interestingly, the NO amounts at the AGM background station also dropped by 31 %; however, the calculated amplitude, between weekdays and Sunday, is two orders of magnitudes smaller (0.04 ppb_v) than at the other sites studied. The latter supports the statement that local anthropogenic sources do not overly influence the AGM station.

Similar reductions are found for NO₂. On average, NO₂ in cities reduces by 23 % during Sundays. The largest amplitude decreases are reported for the most populated cities Nicosia (5.11 ppb_v) and Limassol (4.49 ppb_v), and the smallest, as expected, for the AGM station (0.06 ppb_v). The calculated SO₂ means show a similar tendency with NO and NO₂, with higher weekdays values and lower weekend values. However, the respective decreases are much smaller in amplitudes and percentages. In the cities, SO₂ is, on average, 10 % lower on Sundays. The largest decrease is found for the Mari Industrial site, where a 19 % decrease (0.24 ppb_v) is reported for Sunday. This change could be, to a large extent, explained by the lower consumption of electricity on Sundays because the majority of the industrial and commercial activities cease their operations. At the AGM background station, practically no change is observed between weekdays and the weekend.

An average decline of 9.3 % was observed for CO in the studied cities on Sundays. Measurements at the Nicosia and Limassol curb sites reveal a reduction of 63 and 48 ppb_v, respectively. Smaller-scale reductions are reported for the other cities. Interestingly, in Paphos and Paralimni, CO is slightly higher on Saturdays than on weekdays. This finding could be attributed to the population moving to these regions, mainly for weekend recreation purposes. It is further supported by the observed NO₂ levels that are

also very close to the ones measured on the weekdays. A minimum change in CO, practically negligible, is observed in Agia Marina (CAO) because of the lack of primary anthropogenic sources.

As expected, O₃ increases on the weekend, on average, by 2 ppb_v. The highest increase is found for Nicosia (3.5 ppb_v). This systematic increase emanates most likely from the lower NO levels and the subsequently suppressed destruction of O₃. Similarly, a weekend effect was observed in Eastern Spain (Castell-Balaguer et al., 2012). Due to the negligible NO amounts at the AGM background site, the reported O₃ change is close to zero.

3.4. Diel variability of air pollution in Cyprus

To better understand the mechanisms driving close-to-present ambient pollution in Cyprus, all species' diurnal patterns were calculated using their hourly means (Fig. 4) for 2017–2019. Following the same color coding as before, each type of station is presented with a different color; red for the curb sites (5 stations), orange for the residential (1 station), grey for the industrial (2 stations) and blue for the background (1 station).

The NO and NO₂ at the urban and residential sites present a typical bimodal distribution with morning and evening peaks associated with the transportation/traffic emissions during rush hours. The largest amplitudes in nitrogen oxides are observed for the two largest cities, Nicosia and Limassol. A combination of factors, including lower primary emissions, expansion of the PBL, and photochemical/chemical loss processes, causes the observed noon minimum. An interesting feature observed is the nighttime behavior of the NO variability. Driven by chemistry, the NO levels during the night are expected to be close to zero as NO reacts with O₃ to produce NO₂. During the daytime, NO₂ is photolyzed, forming back NO and regenerating O₃. However, during nighttime, the absence of light does not allow the NO₂ to be photolyzed. As a result, NO is consumed by O₃. As depicted in Fig. 4, the lowest mean nighttime NO mixing ratios at the most populated urban centers reach values up to 5 ppb_v. This observation suggests that elevated localized NO emissions occur at night. This observation is not a unique feature of Cyprus. Elevated nighttime NO levels were observed in several sites in the region, for example, in northeast Italy (Masiol et al., 2017) and a traffic site in South Spain (Notario et al., 2012). Similar behavior characterizes the NO and NO₂ diel variability at the residential site NIC_{RES}, with the amplitude of the peaks being lower than at NIC_{TRA} and the nighttime NO levels being close to zero. The residential site is far away from the key traffic arteries of the city; thus, it is less influenced by direct NO_x emissions. In larger-scale cities and megacities located in the EMME region, elevated NO levels during nighttime have also been reported. In Istanbul, the most populated city in the EMME, the NO amplitude between the early morning minimum and the rush hour peak ranges from 26 to 46 ppb_v, depending on the sampling area within the city (Kasparoglu et al., 2018). A similar range has been observed at traffic stations in this study (up to ~35 ppb_v). However, in Cairo, the second most populated urban agglomeration of the EMME, NO ranges between 80 and 120 ppb_v (Khoder, 2009). For curb stations in Athens, it has also been reported to be 120 ppb_v (Mavroidis and Ilija, 2012).

At the two industrial sites, the magnitude of the diel variability of NO and NO₂ is lower than in the urban ones. The NO₂ at the Zygi site, around 4 km away from the Vasilikos powerplant (PP1), shows a milder urban-type bimodal diurnal variability, possibly due to localized influence from the nearby “Vasilikos” village. Contrary, the NO₂ distribution at the Mari site (1.3 km distance from PP1) shows a trimodal distribution with an additional peak at noon hours. This peak could be attributed to the power plant's operation and the increasing demand for electricity during noon and afternoon (Market Management System for the Cyprus Electricity Market, <https://tsoc.org.cy/electrical-system/>) when the need for air-conditioning use is high. The above assumption is supported by the coincident peak in the diurnal distribution of SO₂ at the Mari station (PP1).

Notably, at the AGM background station, a very weak diurnal NO and NO₂ unimodal variability is observed peaking at noon. The noon peak in NO is most likely caused by local natural temperature-dependent soil emissions (Schindlbacher et al., 2004; Serça et al., 1998; Yienger and Levy II,

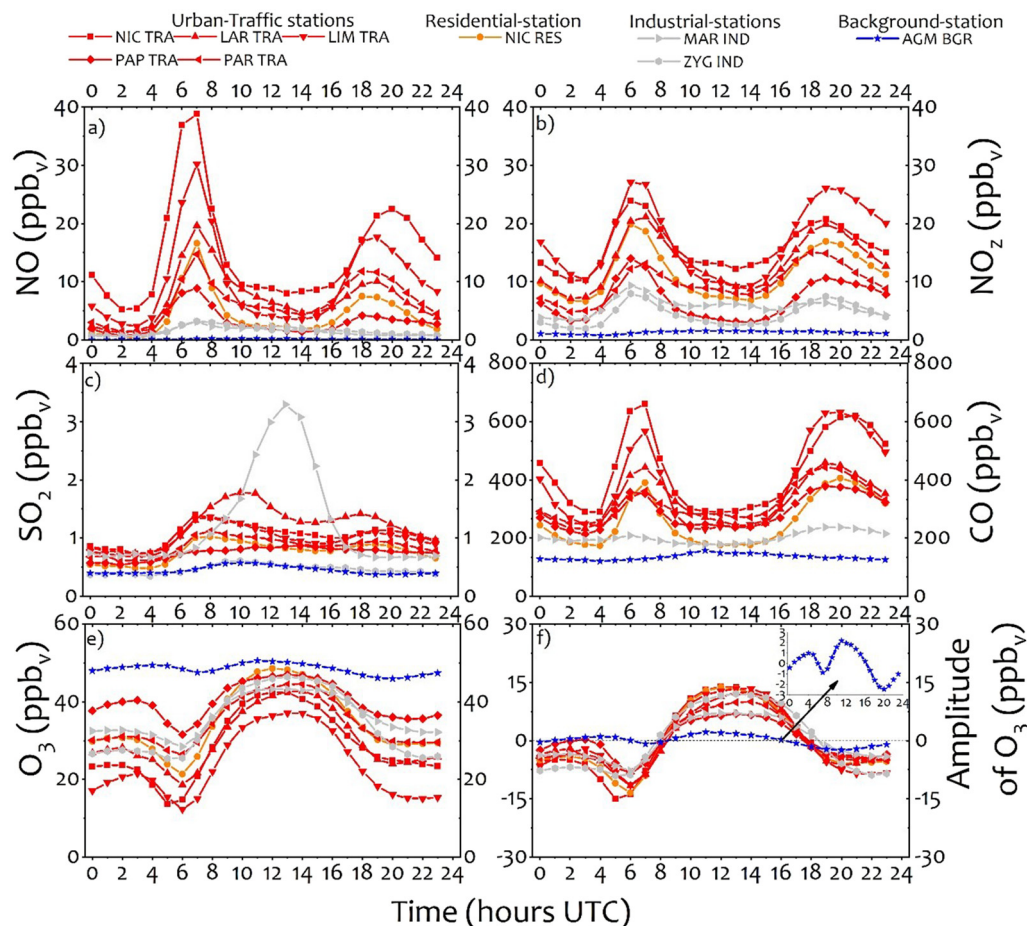


Fig. 4. Diel variability of pollutants (panels a–e) at contrasting environments in Cyprus calculated from the available hourly means of 2017–2019. Panel f shows the amplitude of the ozone mixing ratio compared to its mean daily average.

1995) and the concurrent photolysis of ambient NO₂. That of NO₂ could originate from advected and lofted air masses. Typically, during noon, wind speeds intensify and relative humidity decreases (Kleanthous et al., 2014), allowing both the advection of regional polluted air masses to reach the station and the mixing of air with dryer air masses aloft enriched in long-lived PAN (Singh, 2015) and HNO₃ (Hanke et al., 2003). Both are components of the measured NO_y species.

A distribution almost identical to the one described for NO and NO₂ is observed for the CO daily cycle, with a bimodal curve peaking at the morning and evening rush hours due to traffic-related emissions. The absence of these sources at AGM is visible in its daily cycle of CO, in which there are no increases during the rush hours. Contrary, a small enhancement around noon is found (of ~0.03 ppb_v) due to the enhanced photochemical conditions and the oxidation of local biogenic and regional VOCs (Debevec et al., 2017, 2018).

Moving on to the SO₂ diurnal distribution, most of the stations, except for the Mari industrial one explained before and the AGM station, have a rather weak bimodal daily cycle with morning and evening peaks. On top of emissions related to domestic heating purposes and their apparent influence on the observed SO₂ amounts, the observed pattern seems to be linked with on-road emissions. Similar diel cycles are found for other European cities (Henschel et al., 2013). Once more, these peaks are not observed in the temporal variability of AGM, where a small enhancement (of 0.017 ppb_v) during noon is present, most likely due to intensified convection and the mixing with air masses aloft.

Finally, the O₃ variability pattern presents a common distribution all over the island, with two minima (late morning and evening) and two maxima (early morning and noon). For all stations influenced by anthropogenic

activities, the amplitude of these peaks is larger, with an average noon peak value (up to ~30 ppb_v for the urban centers). A comparable average afternoon peak value (~35 ppb_v) was observed for the sites in the Veneto region (NE Italy), located in the eastern part of the Po Valley (Masiol et al., 2017). Based on the findings of Fig. 4, the following mechanisms are proposed to explain the O₃ cycle: The two minima, at 6:00 and 21:00 UTC, are caused by the ambient NO_x levels, where locally emitted NO reacts with the regionally transported O₃ and destroys it, leading to NO₂ formation. The early morning maximum at 3:00 UTC occurs when the NO levels reach their minimum values, ceasing thus the titration of regionally transported O₃ (Kleanthous et al., 2014). The noon maximum of O₃ at 13:00 UTC is explained by a) the suppressed O₃ destruction due to the drop in NO and NO_y amounts, b) photochemical production controlled by the solar irradiance and the ambient amounts of NO_x and VOCs and c) the rise of the PBL, enabling the mixing with air masses aloft, rich in regional O₃ amounts. At the AGM station, where local anthropogenic emissions are negligible, the overall diurnal variability is weak, and the calculated amplitudes are small and equal to ~2–4 ppb_v.

3.5. Influence of air mass origin on ambient pollutant level

In this analysis, we were restricted by the availability of measurements conducted at all regional background stations simultaneously. From 2011 to 2016, there was an overlap of pollutants data available for all regional background sites, namely the centrally located AGM station, the south-eastern Cavo Greco coastal station, and the western Inia station (Fig. 1). For these 3 stations, median values of NO_y, SO₂, CO and O₃ mixing ratios, wherever available, were computed using the same 6-h temporal step of

the cluster analysis presented before (Section 2.2). The results (Fig. S3) revealed that the most polluted air masses in terms of NO_y , CO and SO_2 mixing ratios originate from the Middle East. The second most polluted cluster, but more important in terms of prevalence, is the SW Asia one. Overall, the absolute average differences between the most polluted masses and the least polluted marine air masses are equal to 0.6, 0.5 and 45 ppb_v for the NO , SO_2 and CO, respectively. An interesting point extracted by the source analysis is that the NO_y at all three background stations is influenced by the air masses' origin, as depicted in the small increases or decreases of the medians. Similar co-variability per cluster is found for CO and SO_2 .

The wind direction is also influencing O_3 . When air originates from Africa or the Middle East or spends a period of at least one day over the sea, the median O_3 level over Cyprus is 46 ppb_v , a value that is 2.2 ppb_v lower than the overall 2011–2016 calculated O_3 median. For the first two clusters, it is known that increased dust loads are associated with decreased O_3 levels (Bonasoni et al., 2004). When air masses originate from polluted West Turkey and SW Asia, the median O_3 is slightly increased, reaching 50 ppb_v . The small changes encountered between the three stations per cluster are likely associated with surface O_3 deposition and chemical formation or destruction from local sources. Notably, the local contribution to O_3 levels computed as the average of the differences between the highest and the lowest O_3 medians is 2.5 ppb_v . This outcome highlights the significant role of regional pollution in the area.

3.6. Local and regional fractions of air pollutants in Cyprus

For this analysis, data from all three environments, namely curb, residential and background stations, are needed to speciate and quantify the fraction of the urban and regional components of air pollution in Cyprus. However, residential observations are only available in Nicosia and Larnaca. In Larnaca, the measurements ended in 2016, while in Nicosia, the dataset included data until 2019. Limited by the above data availability, the last 3 years of the curb and residential data in each city, together with concurrent measurements at the background AGM station, were used. The incentive behind this approach is to present the conditions reflecting the most recent air quality levels. The fractional analysis is based on the calculation of the following components:

- Regional component:** As shown before, the air quality data of the AGM station (X_{BGR}) are representative of the regional contribution of pollution in Cyprus.
- Urban background component:** The difference between the residential and the regional background data, $X_{\text{UBGR}} = X_{\text{RES}} - X_{\text{BGR}}$, where X is NO , NO_z , SO_2 , CO or O_3 , is representative of the localized urban pollution of the city.
- Local – traffic – component:** Since both the curb and the residential sites are influenced by regional pollution, the calculated difference $X_{\text{LOC}} = X_{\text{TRA}} - X_{\text{RES}}$, is representative of the traffic-related pollution in the studied city.

The above three components (X_{LOC} , X_{UBGR} , X_{BGR}) were calculated for all pollutants (Fig. S4) for the two mentioned cities in Cyprus. The findings show that at both curb sites, more than two-thirds of the NO emanates from local-traffic sources (Fig. S4). The remaining third originates from urban background emissions. Interestingly, the NO_z at the curb sites is significantly influenced by urban background emissions that explain 63.6 % and 55 % in Nicosia and Larnaca, respectively. Simultaneously, the regional contribution is estimated to be around 8 %, with the remaining fraction produced by local emissions.

The fractioning of SO_2 and CO seems to be more influenced by regional sources. The regional contribution for the cities of Nicosia and Larnaca is pronounced, accounting for 43 % and 36 % of the SO_2 levels and 31 % and 37 % of the CO levels, respectively. For both cities and the remaining percentage, the urban background contribution to SO_2 and the local-

traffic one to CO dominates. Contrary to the above, urban emissions lead to a total decrease of 29 % of the O_3 levels in the cities, with the highest impact being attributed to local-traffic emissions (~20 %). As explained before, most of the observed O_3 is produced and/or transported regionally.

To better understand the processes linked with the above speciation, a temporal analysis of the seasonal (Fig. S5) variability of the same components is conducted for the city of Nicosia using monthly medians.

The results show that on a year-long basis (Fig. S5), the highest NO urban background fractions (>30 %) are found for the colder winter season when domestic heating emissions maximize. The same is true for the NO_z (>76 %), the SO_2 (39–50 %) and the CO (39–48 %) variability confirming their common emission origin. The contribution of regional emissions is more significant for the summer months for all pollutants. The prevailing northerlies (Kleanthous et al., 2014; Pikridas et al., 2018), bringing polluted air masses from Turkey, SW Asia and, to a lesser extent, Europe, explain this behavior in the region. During the same season, when the overall pollution levels reach their lowest values, the local emissions' contribution to NO , NO_z , and SO_2 is enhanced. This important finding, together with the relatively short lifetime of SO_2 of a few days (von Glasow et al., 2009), reveals that a) either a fraction of the observed SO_2 amounts in Cyprus is produced by traffic-related emissions or b) due to the prevailing northerlies in summer, a localized transport of SO_2 takes place from the northern part of the island. The air mass, in that case, should reach the city of Nicosia without influencing first the AGM background station. Since the reported SO_2 emissions inventories (<https://ec.europa.eu/environment/air/>) for Cyprus exclude the first possibility, the second explanation seems to be the most likely candidate for the above observation. Notably, the satellite-based analysis of the tropospheric NO_2 spatial variability (see Section 3.8) reveals that the powerplant PP5 (see Fig. 1) is the strongest polluter on the island. This SO_2 emission source corroborates the above hypothesis. The passage created between the Pentadaktylos and Troodos Mountain complexes facilitates air masses' transport from PP5 towards the NIC_{TRA} site in summer. Lastly, and as expected, the high urban NO_z emissions have an important influence on the observed winter O_3 levels, with up to 40 % of O_3 (24–31 ppb_v) being titrated. During the summer, the overall sink mechanism has a reduced effect removing up to 19 % of O_3 (12–13 ppb_v).

The lack of residential data for the rest of the cities does not allow for a similar analysis for all urban centers. Nonetheless, an estimation of the total urban contribution (X_{URB}) from the curb and regional differences ($X_{\text{TRA}} - X_{\text{BGR}}$) is possible. Using the X_{URB} and the X_{BGR} information, the NO , NO_z , SO_2 , CO and O_3 amounts of 2017–2019 were split into their urban and regional components (Fig. 5). The results show that the five cities of the study can be divided into two groups; the three largest cities (Nicosia, Larnaca, and Limassol; group A) are influenced more by local urban contributions than the other two cities (Paralimni and Paphos; group B). The largest O_3 titration in group A (average loss of 30 %), compared to group B (19 %), corroborates the above finding.

3.7. Chemical clocks

[CO-to- NO_y ratio]: The above data, when used in the form of ratios, often referred to as chemical clocks, can reveal additional information on the spatial characteristics of pollution. One of these is the CO-to- NO_x (or, in our case NO_y) ratio. Due to the different time scales of the lifetime of CO (~1–2 months) and the NO_x (and NO_y ; hours to few days), CO can stay much longer in the atmosphere (Parrish et al., 2009). As a result, urban CO amounts are more prone to being affected by upwind regional CO sources than the shorter-lived odd nitrogen oxides. Cities with significant localized emissions have a CO: NO_x ratio close to 10, or even less, while for remote places, this ratio often exceeds the value of 80 (Kanakidou et al., 2011; Parrish, 2006; Parrish et al., 2009). Some examples described in the studies mentioned above include the city of Mexico (ratio = 11), Tokyo (8.5), Los Angeles (9.7), Atlanta (6.5), Athens (20–30), the city of Beijing (45) and the Finokalia rural station in Crete, Greece (100–300). In the case of Beijing, the city was influenced by regional upwind biomass

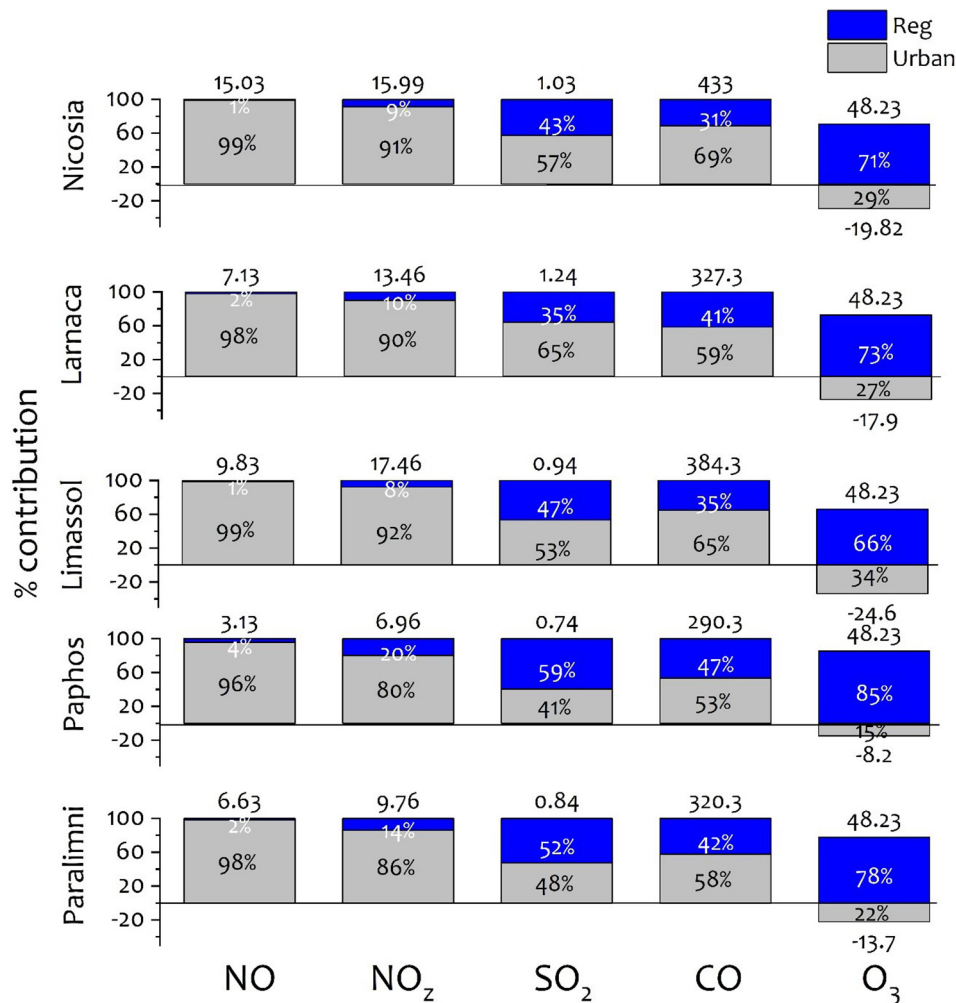


Fig. 5. Partitioning of urban and regional pollution levels in all cities (2017–2019) using as a regional reference the ambient pollutant levels at the CAO station.

burning sources rich in CO (Parrish et al., 2009). The analysis of the annual CO-NO_y ratios for all sites in Cyprus (Fig. S6), where concurrent CO and NO_y data exist, shows that the curb sites of Nicosia (CO-to-NO_y ratio = 13.65 ± 5.57), Larnaca (15.97 ± 5.16), Limassol (14.10 ± 4.79), Paralimni (19.58 ± 7.38) as well as the residential Nicosia site (16.74 ± 5.16) seem to be impacted by local pollution. Regional influences are more pronounced for the residential Larnaca site (24.57 ± 8.19), the city of Paphos (29.03 ± 13.24), and the Mari industrial station (28.00 ± 8.38). Finally, as was the case of the Finokalia rural station, the AGM station exhibits the highest ratio (90.79 ± 27.08); thus, as expected, it is strongly influenced by transported air masses.

[O₃-to-NO_y ratio]: To assess the titration impact of the total odd nitrogen oxides on the O₃ levels in Cyprus, all available NO_y and O₃ annual data were used to investigate the spatial variation in the O₃-NO_y relationship. For that purpose, data without any temporal filters (i.e. including daytime and nighttime values) have been used. The analysis (Fig. 6) shows that the majority of the dataset lies on the logarithmic fit:

$$[O_3] = -7.7 \ln ([NO_y] + 0.36) + 53.03, \text{ with } R^2 = 0.88 \quad (1)$$

The observed fit denotes that the behavior of the NO_y-O₃ system is non-linear, as it is widely reported in the literature (e.g., Seinfeld and Pandis, 2006). This nonlinearity is one of the main reasons that alleviating O₃ pollution remains a challenging task. Towards this direction, the same O₃-to-NO_y ratio has been proposed to serve as an indicator of the photochemical O₃-NO_x-VOC sensitivity (Sillman and He, 2002; Trainer, 1993). In the NO_x limited regime, where ambient NO_x levels are low and VOCs high, O₃ is

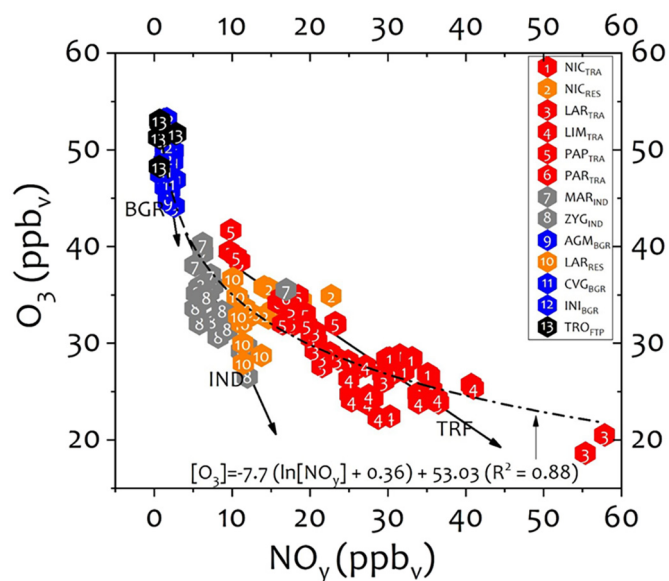


Fig. 6. Ozone-to-NO_y ratios calculated using all available annual O₃ and NO_y mean values from the thirteen monitoring stations of Cyprus.

mainly controlled by NO_x changes. On the other hand, in VOC limited regimes with high NO_x and low VOCs, O₃ increases with increasing VOCs and decreases for higher NO_x. This differentiation is, therefore, crucial for policymaking decisions. Depending on the environment, this ratio can be used to characterize the studied regions as NO_x or VOC limited (Carrillo-Torres et al., 2017; and references therein). When the O₃:NO_y lies below 11, for regions with O₃ levels lower than 80 ppbv, (as is the case of all sites in Cyprus), the region is VOC limited, and for ratios higher than 15, NO_x limited.

The computed ratios using all available annual averages, filtered to include only daytime hours (10–16 LT), are depicted in Fig. 7. Interestingly, for the sites affected by anthropogenic activities, the mean O₃:NO_y ratio was equal to 4.48 ± 0.44, whereas for the regional background stations Agia Marina, Cavo Greco and Inia, the ratio was 27.8 ± 2.2. The ratio at the free troposphere Troodos site presents the highest value of 49.1 ± 4.3. Based on the threshold mentioned above, the urban, residential and industrial sites are NO_x saturated and VOC limited areas. The remaining four sites are NO_x limited. This finding shows that the increasing trends observed in O₃ levels in cities (Section 3.1), despite pollution control strategies targeting the reduction of NO_x, are possibly caused by the presence of VOCs. The latter highlights the need for designing tailored policies to the needs of each agglomeration.

3.8. A view from space – tropospheric NO₂ variability

The above results were based on the availability of data acquired at specific geolocations. To overcome spatial limitations, the distribution of pollution over Cyprus has been analyzed using satellite data. For that purpose, observations of NO₂ have been chosen because of its short lifetime that allows its detection close to emission sources due to limited transport controlled by ambient meteorological conditions. The analysis is based on NO₂ data from the TROPOspheric Monitoring Instrument (TROPOMI) onboard the European Copernicus Sentinel 5 Precursor (S5P) (Veefkind et al., 2012). S5P provides a daily overpass at around 13:30LT with a spatial nadir resolution of 7 km × 3.5 km (5.5 km × 3.5 km since August 2019) that ultimately allows for detecting NO₂ at a city level (e.g., Ialongo et al., 2019). The results are expressed in vertical column densities (VCDs) and molecules per square centimeter (molec cm⁻²).

The results show the average distribution of the VCD_{NO2} for 2019 over the Eastern Mediterranean region (Fig. 8a) and Cyprus (Fig. 8b). The year 2019 was selected because it is the first calendar year where TROPOMI data are available. On a regional scale, high levels of NO₂ are confined over the neighboring countries of Cyprus, including Egypt, Israel, Lebanon and Turkey. These NO_x emissions are indicative of fossil fuel energy consumption. Due to their common sources, it is expected that enhanced emissions of long-lived CO would accompany the NO_x emissions. The latter can be transported, during favorable meteorological conditions, towards Cyprus.

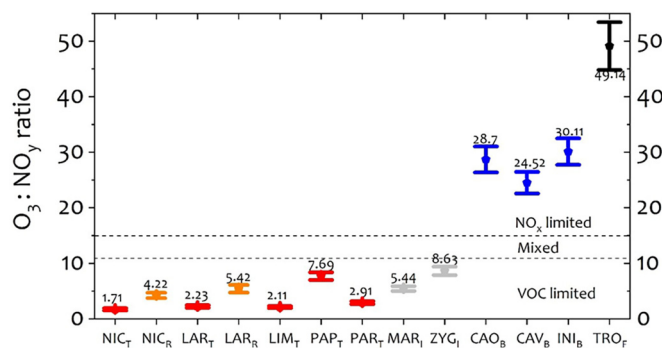


Fig. 7. Ozone-to-NO_y computed ratios using all available annual averages at all monitoring stations but filtered to include only daytime hours (10–16 LT). The dashed lines separate the fractions into VOC-limited, mixed and NO_x-limited ranges.

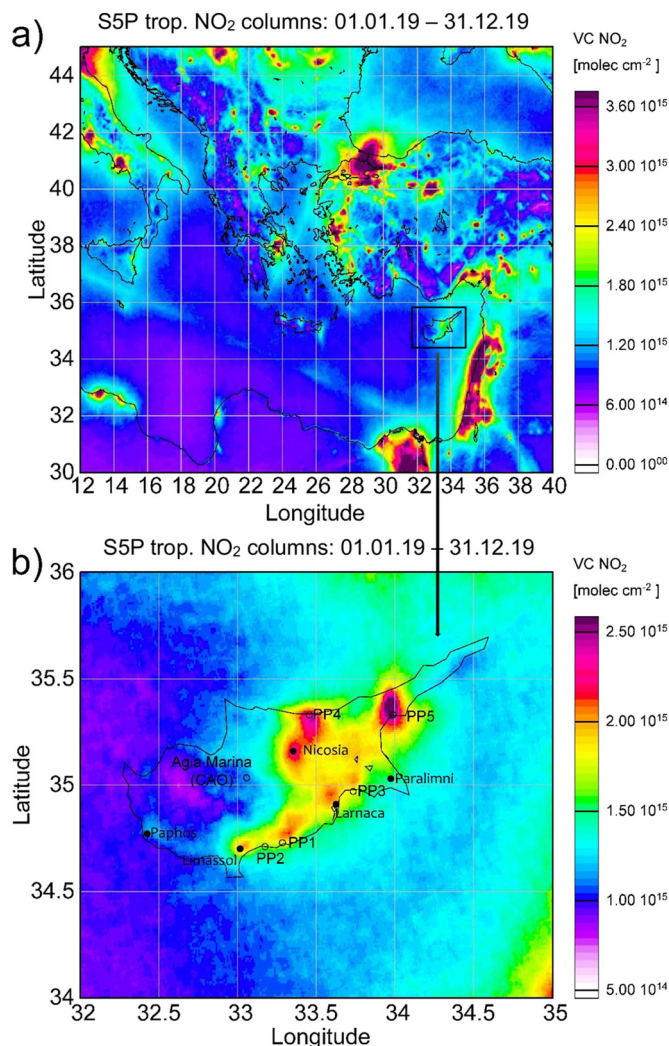


Fig. 8. Spatial variability of space-based (S5P-TROPOMI) vertical columns of NO₂ in 2019, in the East Mediterranean (panel a) and Cyprus (panel b) regions. Panel b embeds the geolocation of the main urban centers and powerplants in Cyprus and the location of the background station CAO.

The analysis reveals a clear geographic west-east low-to-high gradient of the VCD_{NO2} spatial distribution over Cyprus (Fig. 8b). When comparing the NO₂ hotspots with the location of powerplants (Fig. 1), it is evident that powerplant NO_x emissions are the dominant ones in Cyprus. Overall, the PP₅ (175 MW, heavy oil) and PP₄ (362 MW, heavy oil & natural gas) facilities located in the north of the island are the principal sources of NO₂ for the studied period, followed by PP₁ (868 MW, heavy fuel & natural gas), PP₂ (460 MW, heavy fuel) and PP₃ (150 MW, heavy fuel) ones. Interestingly, the observed pollution strength of the PPs, in terms of NO₂ amounts, is not proportional to their operating capacity possibly pointing to less efficient pollution control technologies applied for the cases of PP₄ and PP₅.

In addition to the powerplant emissions, all major cities on the island are visible from space. On average, the NO₂ VCD amounts over cities are around 2–4 times higher than the background levels of the island (~5·10¹⁴ molec·cm⁻²).

By applying SOM, NO₂ pollution sources, shown in Fig. 8b, are identified and isolated from their surroundings by the algorithm. For example, the PP₅ source in the northeast of Cyprus is assigned to separate clusters in all 4 SOM sensitivity tests (9, 12, 16, and 20 clusters; Fig. S7). The difference between the tests (and the number of clusters, respectively) is the level of isolation of each plume. In the example with 9 clusters, 2 sub-clusters are dedicated to source PP₅. In the example with 12 clusters, it is 3, with 16 and

20 clusters it is 4. However, since the magnitude of the NO₂ column was the only input parameter to the SOM algorithm, different areas/sources could be assigned to the same cluster, as is the case in the SOM panel with 12 clusters for the PP4 and Nicosia areas. However, this behavior is not considered a drawback because the point of implementing the SOM algorithm was to identify all sources of enhanced NO₂ and estimate their contribution to the total NO₂ over Cyprus.

The contribution of each plume was quantified by adding the NO₂ columns contained in clusters that represent the same source. In cases similar to the example described above (i.e., when two distinct sources belong to the same cluster), we calculated the contribution of each source separately. This contribution is then normalized to the total NO₂ column of Cyprus for 2019 (Table 3). From these results, the overall contribution of all sources and cities is inferred. Interestingly, it is shown that local sources from powerplants and cities do not contribute significantly (i.e., around 10 %) to the overall tropospheric NO₂ columns over Cyprus.

4. Summary and conclusions

Cyprus is centrally located in the East Mediterranean and Middle East (EMME) region and at the crossroad of three continents, namely Europe, Africa and Asia. It is influenced by transported anthropogenic emissions emanating from Europe, Asia and the Middle East, and natural dust emissions from Africa and the Middle East (Kleanthous et al., 2014). This long-range transport of pollution, together with local emissions due to anthropogenic activities such as traffic and power consumption and natural processes such as wildfires and dust resuspension, degrades the air quality over the island. Overall, local and regional air pollution in Cyprus and the broader EMME region is identified as a challenging environmental problem (e.g., Kanakidou et al., 2011) with O₃ (Kleanthous et al., 2014) and aerosol (Pikridas et al., 2018) concentration thresholds being frequently exceeded. These exceedances and the subsequent poor air quality have a negative impact on the health of the population in the EMME region (~400 M people).

To better assess the temporal variability of air pollution in Cyprus, we presented and discussed the longest dataset, to our knowledge, of gaseous trace pollutants and one of the longest for EMME, covering a span of 17 years (2003–2019). Additionally, to tackle the spatial variability of pollution, we introduced in the analysis data from different environments covering curb monitoring sites operating at the largest cities of the island, along with residential, industrial, background and free-troposphere monitoring stations.

In brief, the results showed the following:

- The daily data showed that the background NO and NO₂ median values of ~0.15 ppb_v are two orders of magnitude lower than in cities. At the same time, CO median values are four times lower at the regional Agia Marina (CAO) station (130 ppb_v) than in the larger scale Nicosia, Limassol and Larnaca cities, showing that local pollution is not

negligible. Regarding SO₂, the highest median values are found for the industrial Mari station (~1.3 ppb_v), which is placed close to a large powerplant (PP1) and the city of Limassol (1.25 ppb_v), which hosts the largest commercial port of the island but is also frequently found downwind the plume of the powerplant mentioned above. Relatively low O₃ median mixing ratios are recorded in the cities (~25 ppb_v), whereas at the background and free troposphere stations, the respective value is twice as high. Notably, high O₃ values are found in the whole EMME region controlled by synoptic meteorology, enhanced insolation and the proximity of precursor species' emissions.

- The multiannual analysis performed at eight stations with more than ten years of data using the Mann-Kendall trend analysis revealed for all pollutants except O₃, a decreasing trend. In contrast, at four out of the eight monitoring stations, a statistically significant increase in O₃ levels is found, ranging between 0.36 ppb_v y⁻¹ (ZYG_{IND}) and 0.82 ppb_v y⁻¹ (LAR_{RES}). The latter can be explained by the O₃:NO_y ratio analysis that suggested that these regions lie in the VOC-limited regime where a decrease in NO_x amounts due to mitigation strategies can lead to an increase in O₃.
- The NO and NO_z (for this study NO_z = NO_y - NO) interannual variability was unimodal, with the higher values being found for winter. Despite the longer lifetime of CO than NO_x, CO behavior was similar to NO and NO_z with an additional smaller scale peak observed in summer explained by i) the CO transported regionally to the island during the prevailing northerlies and ii) the production of CO from the oxidation of VOCs. For the SO₂, smaller-scale seasonal variability was observed in most sites, with winter-to-summer high-to-low values explained by domestic heating. However, the industrial Mari station presents an opposite variability with the peak observed in summer. The increased power production from the neighboring powerplant can explain this difference.
- Regarding O₃, in the majority of the sites, the highest values are found in summer, and the lowest in winter, mostly due to a) its enhanced photochemical production during high insolation and b) the transport of air mass advected from long distances. The interannual variability of O₃ at the background station Agia Marina, where local NO_z and CO amounts are very low, supports the latter. Notably, at the industrial stations Mari and Zygi, the winter-to-summer O₃ amplitude is much smaller. One possibility is that this is caused by acid displacement mechanisms taking place in coastal regions where sulfates enable the release of chlorine radicals that attack O₃ molecules.
- The diurnal variability of major pollutants in Cyprus calculated from hourly means showed the local emissions' footprint in cities. This behavior is evident from the diurnal variability of NO, NO_z and CO, where high amplitude peaks are visible in the morning and evening associated with transportation emissions during rush hour. A very weak bimodal rush-hour oriented distribution of values is also observed for SO₂, suggesting a smaller scale contribution of on-road emissions. Lastly, O₃ at all monitoring sites presents a characteristic shape with two minima and two maxima controlled by chemical titration with NO_x, photochemical production and regional O₃ transport. At the same time, the amplitude of the diel variability of O₃ at the background Agia Marina station is very small due to the absence of local anthropogenic emissions.
- The speciation and quantification of the contribution of local traffic, urban-background and regional components of pollution in Nicosia and Larnaca cities suggest that, on average, for both cities, 99 % of NO emanates from traffic and urban background sources. The same is true for 92 % of the NO_z. On the other hand, almost 40 % of SO₂ and 34 % of CO originate from regionally transported sources. Interestingly, 29 % of O₃ seems to be depleted in cities, with the rest being transported and/or formed regionally.
- The CO-to-NO_y ratio was used to assess the regional vs. local character of pollution in Cyprus. The analysis showed that the curb sites and the residential stations are influenced, to a large extent, by local pollution, with the computed CO:NO_y ratio being equal to ~15, while the Agia Marina station is mostly regionally influenced, with a ratio of 90.

Table 3

Contribution of each source or city to the total pollution of Cyprus for 2019. Each column indicates the contribution (in percentage and number of clusters) of each source or city, depending on the number of clusters used. The last column (ensemble) is the average of all the four sensitivity tests, while the last line estimates the total contribution in NO₂ pollution from all sources of each sensitivity test.

Sources	Number of clusters (# of clusters used in each calculation)				Ensembles
	9	12	16	20	
PP5	3.73 % (2)	4.00 % (3)	3.14 % (3)	3.71 % (4)	3.65 %
PP4	3.18 % (2)	1.67 % (1)	2.32 % (2)	1.90 % (2)	2.27 %
Nicosia	2.77 % (1)	0.68 % (1)	1.60 % (2)	0.95 % (1)	1.5 %
PP3	0.13 % (1)	0.29 % (1)	0.29 % (1)	1.68 % (2)	0.60 %
Larnaca	0.80 % (1)	1.11 % (1)	1.11 % (2)	1.77 % (2)	1.20 %
PP1	0.75 % (1)	1.04 % (1)	1.02 % (2)	1.75 % (2)	1.14 %
Limassol	0.86 % (2)	0.60 % (2)	0.87 % (3)	0.61 % (3)	0.73 %
Paphos	0.20 % (1)	0.04 % (1)	0.71 % (2)	0.66 % (2)	0.40 %
Summation	12.42 %	9.43 %	11.06 %	13.03 %	11.48 %

- The computed O_3 -to- NO_y ratio indicates that the background and the free-troposphere stations can be characterized as NO_x -limited, with the respective ratios being in the range of 24.5 to 49.1. The urban centers, residential sites and industrial sites are VOC-limited, with ranges between 1.7 and 8.6. The latter is important when planning pollution control strategies that target O_3 reduction. In that case, control actions targeting simultaneously NO_x and VOC reductions are needed.
- Lastly, satellite data of tropospheric NO_2 vertical columns revealed a west-east low-to-high gradient over the island. All major hotspots, including cities and powerplants, are visible from space. When compared, the observed NO_2 pollution from powerplants is not proportional to their operating capacity pointing to less efficient pollution control strategies for the two powerplants (PP_4 and PP_5) found in the north of the island.
- Interestingly, a machine-based clustering analysis enabled the quantification of each hotspot plume and, subsequently, its contribution to the sum of NO_2 pollution sources over Cyprus. The results revealed that all major cities and powerplants combined contribute overall only around 10 % to the tropospheric NO_2 columnar amounts in Cyprus. The rest emanates from other local sources, and from the regional NO_2 levels confined from the neighboring countries Egypt, Israel, Lebanon and Turkey, as seen from the NO_2 distribution over the East Mediterranean region.

CRedit authorship contribution statement

M. Vrekoussis: Conceptualization, Methodology, Formal analysis, Writing – original draft, Visualization, Investigation, Supervision. **M. Pikridas:** Software, Formal analysis, Writing – review & editing. **C. Rousogenous:** Methodology, Writing – review & editing. **A. Christodoulou:** Methodology, Writing – review & editing. **M. Desservettaz:** Methodology, Writing – review & editing. **J. Sciare:** Funding acquisition, Writing – review & editing, Supervision. **A. Richter:** Resources, Methodology, Formal analysis, Writing – review & editing. **I. Bougoudis:** Resources, Methodology, Formal analysis, Writing – review & editing. **C. Savvides:** Resources, Writing – review & editing. **C. Papadopoulos:** Resources, Writing – review & editing.

Declaration of competing interest

The authors declare that they have no known competing financial interests or personal relationships that could have appeared to influence the work reported in this paper.

Acknowledgments

The authors would like to thank the personnel of the Air Quality Section of the Department of Labour Inspection (DLI) for providing filters and air quality parameters. This paper contains modified Copernicus Sentinel data processed at IUP Bremen. The authors thank EU/ESA/KNMI/DLR for providing the TROPOMI/S5P level 1 and level 2 products. This study has been financially supported by the H2020-EMME-CARE (GA 856612) research grant. MV acknowledges financial support from the co-funded DFG-NSFC Sino-German AirChanges project (448720203).

Appendix A. Supplementary data

Supplementary data to this article can be found online at <https://doi.org/10.1016/j.scitotenv.2022.157315>.

References

Aas, W., Mortier, A., Bowersox, V., Cherian, R., Faluvegi, G., Fagerli, H., Hand, J.L., Klimont, Z., Galy-Lacaux, C., Lehmann, C.M.B., Myhre, C.L., Myhre, G., Olivie, D., Sato, K., Quaas, J., Rao, P.S.P., Schulz, M., Shindell, D.T., Skeie, R.B., Stein, A., Takemura, T., Tsyro, S., Vet, R., Xu, X., 2019. Global and regional trends of atmospheric sulfur. *Sci. Rep.* 9, 953. <https://doi.org/10.1038/s41598-018-37304-0>.

Adame, J.A., Sole, J.G., 2013. Surface ozone variations at a rural area in the northeast of the Iberian Peninsula. *Atmos. Pollut. Res.* 4 (2), 130–141. <https://doi.org/10.5094/APR.2013.013>.

Aff, C., Chélala, C., Borbon, A., Abboud, M., Adjizian-Gérard, J., Farah, W., Jambert, C., Zaarour, R., Saliba, N.B., Perros, P.E., Rizk, T., 2008. SO_2 in Beirut: air quality implication and effects of local emissions and long-range transport. *Air Qual. Atmos. Health* 1 (3), 167–178. <https://doi.org/10.1007/s11869-008-0022-y>.

Aff, C., Dutot, A.L., Jambert, C., Abboud, M., Adjizian-Gérard, J., Farah, W., Perros, P.E., Rizk, T., 2009. Statistical approach for the characterization of NO_2 concentrations in Beirut. *Air Qual. Atmos. Health* 2 (2), 57–67. <https://doi.org/10.1007/s11869-009-0034-2>.

Al-Jeelani, H.A., 2009. Air quality assessment at Al-Taneem area in the Holy Makkah City Saudi Arabia. *Environ. Monit. Assess.* 156 (1–4), 211–222. <https://doi.org/10.1007/s10661-008-0475-3>.

Al-Jeelani, H.A., 2014. Diurnal and seasonal variations of surface ozone and its precursors in the atmosphere of Yanbu, Saudi Arabia. *J. Environ. Prot.* 05 (05), 408–422. <https://doi.org/10.4236/jep.2014.55044>.

Bonasoni, P., Cristofanelli, P., Calzolari, F., Bonafè, U., Evangelisti, F., Stohl, A., Sajani, S.Z., Van Dingenen, R., Colombo, T., Balkanski, Y., 2004. Atmospheric chemistry and physics aerosol-ozone correlations during dust transport episodes. *Atmos. Chem. Phys.* 4. www.atmos-chem-phys.org/acp/4/1201/.

Bougoudis, I., Demertzis, K., Iliadis, L., 2016. HISYCOL: a hybrid computational intelligence system for combined machine learning: the case of air pollution modeling in Athens. *Neural Comput. Appl.* 2016 (27), 1191–1206.

Buringh, E., Fischer, P., Hoek, G., 2000. Is SO_2 a causative factor for the PM-associated mortality risks in the Netherlands? *Inhal. Toxicol.* 12 (sup1), 55–60. <https://doi.org/10.1080/0895-8378.1987.11463181>.

Burnett, R.T., Stieb, D., Brook, J.R., Cakmak, S., Dales, R., Raizenne, M., Vincent, R., Dann, T., 2004. Associations between short-term changes in nitrogen dioxide and mortality in Canadian cities. *Arch. Environ. Health* 59 (5), 228–236. <https://doi.org/10.3200/AEOH.59.5.228-236>.

Carrillo-Torres, E., Hernández-Paniagua, I., Mendoza, A., 2017. Use of combined observational- and model-derived photochemical indicators to assess the O_3 - NO_x -VOC system sensitivity in urban areas. *Atmosphere* 8 (12), 22. <https://doi.org/10.3390/atmos8020022>.

Castellanos, P., Boersma, K.F., 2012. Reductions in nitrogen oxides over Europe driven by environmental policy and economic recession. *Sci. Rep.* 2 (1), 265. <https://doi.org/10.1038/srep00265>.

Castell-Balaguer, N., Téllez, L., Mantilla, E., 2012. Daily, seasonal and monthly variations in ozone levels recorded at the turia river basin in Valencia (Eastern Spain). *Environ. Sci. Pollut. Res.* 19 (8), 3461–3480. <https://doi.org/10.1007/s11356-012-0881-5>.

Cerro, J.C., Cerdà, V., Pey, J., 2015. Trends of air pollution in the Western Mediterranean Basin from a 13-year database: a research considering regional, suburban and urban environments in mallorca (Balearic Islands). *Atmos. Environ.* 103, 138–146. <https://doi.org/10.1016/j.atmosenv.2014.12.014>.

Cerro, José C., Cerdà, V., Querol, X., Alastuey, A., Bujosa, C., Pey, J., 2020. Variability of air pollutants, and PM composition and sources at a regional background site in the Balearic Islands: review of western Mediterranean phenomenology from a 3-year study. *Sci. Total Environ.* 717, 137177. <https://doi.org/10.1016/j.scitotenv.2020.137177>.

Chang, C.Y., Faust, E., Hou, X., Lee, P., Kim, H.C., Hedquist, B.C., Liao, K.J., 2016. Investigating ambient ozone formation regimes in neighboring cities of shale plays in the Northeast United States using photochemical modeling and satellite retrievals. *Atmos. Environ.* 142, 152–170. <https://doi.org/10.1016/j.atmosenv.2016.06.058>.

Chiusolo, M., Cadum, E., Stafoggia, M., Galassi, C., Berti, G., Faustini, A., Bisanti, L., Vigotti, M.A., Dessì, M.P., Cernigliaro, A., Mallone, S., Pacelli, B., Minerba, S., Simonato, L., Forastiere, F., EpiAir Collaborative Group, 2011. Short-term effects of nitrogen dioxide on mortality and susceptibility factors in 10 Italian cities: the EpiAir study. *Environ. Health Perspect.* 119 (9), 1233–1238. <https://doi.org/10.1289/ehp.1002904> Sep.

Cole, M.A., 2003. Development, Trade, and the Environment: How Robust is the Environmental Kuznets Curve?

Crutzen, P.J., 1979. The role of NO and NO_2 in the chemistry of the troposphere and stratosphere. *Annu. Rev. Earth Planet. Sci.* 7, 443–472.

Cuevas, C.A., Notario, A., Adame, J.A., Hilboll, A., Richter, A., Burrows, J.P., Saiz-Lopez, A., 2014. Evolution of NO_2 levels in Spain from 1996 to 2012. *Sci. Rep.* 4 (2), 1–8. <https://doi.org/10.1038/srep05887>.

Dayan, U., Ricaud, P., Zbinden, R., Dulac, F., 2017. Atmospheric pollution over the eastern Mediterranean during summer – a review. *Atmos. Chem. Phys.* 17, 13233–13263. <https://doi.org/10.5194/acp-17-13233-2017>.

Debevec, Cécile, Sauvage, S., Gros, V., Sciare, J., Pikridas, M., Stavroulas, I., Salameh, T., Leonardis, T., Gaudion, V., Depelchin, L., Fronval, I., Sarda-Estève, R., Baisnée, D., Bonsang, B., Savvides, C., Vrekoussis, M., Locoge, N., 2017. Origin and variability in volatile organic compounds observed at an eastern Mediterranean background site (Cyprus). *Atmos. Chem. Phys.* 17 (18), 11355–11388. <https://doi.org/10.5194/acp-17-11355-2017>.

Debevec, Cécile, Sauvage, S., Gros, V., Sellegri, K., Sciare, J., Pikridas, M., Stavroulas, I., Leonardis, T., Gaudion, V., Depelchin, L., Fronval, I., Sarda-Estève, R., Baisnée, D., Bonsang, B., Savvides, C., Vrekoussis, M., Locoge, N., 2018. Driving parameters of biogenic volatile organic compounds and consequences on new particle formation observed at an eastern Mediterranean background site. *Atmos. Chem. Phys.* 18 (19), 14297–14325. <https://doi.org/10.5194/acp-18-14297-2018>.

Eger, P.G., Friedrich, N., Schuladen, J., Shenolikar, J., Fischer, H., Tadic, I., Harder, H., Martinez, M., Rohloff, R., Tauer, S., Drewnick, F., Fachinger, F., Brooks, J., Darbyshire, E., Sciare, J., Pikridas, M., Lelieveld, J., Crowley, J.N., 2019. Shipborne measurements of $CINO_2$ in the Mediterranean Sea and around the arabian peninsula during summer. *Atmos. Chem. Phys.* 19 (19), 12121–12140. <https://doi.org/10.5194/acp-19-12121-2019>.

- European Environmental Agency, 2018. EEA Report No 12/2018. Issue 12Vol. 12. <https://www.eea.europa.eu/publications/air-quality-in-europe-2018/download>.
- Falcieri, F.M., Benetazzo, A., Scavo, M., Russo, A., Carniel, S., 2014. Po River plume pattern variability investigated from model data. *Cont. Shelf Res.* 87, 84–95. <https://doi.org/10.1016/j.csr.2013.11.001>.
- Farah, W., Nakhlé, M.M., Abboud, M., Annesi-Maesano, I., Zaarour, R., Saliba, N., Germanos, G., Gerard, J., 2014. Time series analysis of air pollutants in Beirut, Lebanon. *Environ. Monit. Assess.* 186 (12), 8203–8213. <https://doi.org/10.1007/s10661-014-3998-9>.
- Forster, P.M., Bodeker, G., Schofield, R., Solomon, S., Thompson, D., 2007. Effects of ozone cooling in the tropical lower stratosphere and upper troposphere. *Geophys. Res. Lett.* 34 (23). <https://doi.org/10.1029/2007GL031994> n/a-n/a.
- Gaudel, A., Cooper, O.R., Ancellet, G., Barret, B., Boynard, A., Burrows, J.P., Clerbaux, C., Coheur, P.-F., Cuesta, J., Cuevas, E., Doniki, S., Dufour, G., Ebojje, F., Foret, G., Garcia, O., Granados-Muñoz, M.J., Hannigan, J.W., Hase, F., Hassler, B., Ziemke, J., 2018. Tropospheric ozone assessment report: present-day distribution and trends of tropospheric ozone relevant to climate and global atmospheric chemistry model evaluation. *Elementa (Wash. D.C.)*, 6 <https://doi.org/10.1525/elementa.291>.
- Gerasopoulos, E., Kouvarakis, G., Vrekoussis, M., Kanakidou, M., Mihalopoulos, N., 2005. Ozone variability in the marine boundary layer of the eastern Mediterranean based on 7-year observations. *J. Geophys. Res. D: Atmos.* 110 (15), 1–12. <https://doi.org/10.1029/2005JD005991>.
- Gerasopoulos, Evangelos, Kouvarakis, G., Vrekoussis, M., Donoussis, C., Mihalopoulos, N., Kanakidou, M., 2006. Photochemical ozone production in the eastern Mediterranean. *Atmos. Environ.* 40 (17), 3057–3069. <https://doi.org/10.1016/j.atmosenv.2005.12.061>.
- Gilbert, 1987. Statistical methods for environmental pollution monitoring. Wiley. <https://www.wiley.com/en-us/Statistical+Methods+for+Environmental+Pollution+Monitoring-p-9780471288787>.
- Guerreiro, C.B.B., Foltescu, V., de Leeuw, F., 2014. Air quality status and trends in Europe. *Atmos. Environ.* 98, 376–384. <https://doi.org/10.1016/j.atmosenv.2014.09.017>.
- Hanke, M., Umann, B., Uecker, J., Arnold, F., Bunz, H., 2003. Atmospheric Chemistry and Physics Atmospheric measurements of gas-phase HNO₃ and SO₂ using chemical ionization mass spectrometry during the MINATROC field campaign 2000 on Monte Cimone. *Atmos. Chem. Phys.* 3. www.atmos-chem-phys.org/acp/3/417/.
- Haykin, S., 1999. *Neural Networks: A Comprehensive Foundation*. Prentice Hall.
- Henschel, S., Querol, X., Atkinson, R., Pandolfi, M., Zeka, A., Le Tertre, A., Analitis, A., Katsouyanni, K., Chanel, O., Pascal, M., Boulard, C., Haluza, D., Medina, S., Goodman, P.G., 2013. Ambient air SO₂ patterns in 6 European cities. *Atmos. Environ.* 79, 236–247. <https://doi.org/10.1016/j.atmosenv.2013.06.008>.
- Hesterberg, T.W., Bunn, W.B., McClellan, R.O., Hamade, A.K., Long, C.M., Valberg, P.A., 2009. Critical review of the human data on short-term nitrogen dioxide (NO₂) exposures: evidence for NO₂ no-effect levels. *Crit. Rev. Toxicol.* 39 (9), 743–781. <https://doi.org/10.3109/10408440903294945>.
- Ialongo, I., Virta, H., Eskes, H., Hovila, J., Douros, J., 2019. Comparison of TROPOMI/Sentinel 5 Precursor NO₂ Observations With Ground-Based Measurements in Helsinki. <https://doi.org/10.5194/amt-2019-329>.
- Jaeglé, L., Steinberger, L., Martin, R.V., Chance, K., 2005. Global partitioning of NO_x sources using satellite observations: relative roles of fossil fuel combustion, biomass burning and soil emissions. *Faraday Discuss.* 130, 407. <https://doi.org/10.1039/b502128f>.
- Kalabokas, P.D., Repapis, C.C., 2004. A climatological study of rural surface ozone in Central Greece. *Atmos. Chem. Phys.* 4 (4), 1139–1147. <https://doi.org/10.5194/acp-4-1139-2004>.
- Kalabokas, P.D., Viras, L.G., Bartzis, J.G., Repapis, C.C., 2000. Mediterranean rural ozone characteristics around the city of Athens. *Atmos. Environ.* 34 (29–30), 5199–5208. [https://doi.org/10.1016/S1352-2310\(00\)00298-3](https://doi.org/10.1016/S1352-2310(00)00298-3).
- Kalabokas, P.D., Mihalopoulos, N., Ellul, R., Kleanthous, S., Repapis, C.C., 2008. An investigation of the meteorological and photochemical factors influencing the background rural and marine surface ozone levels in the central and eastern Mediterranean. *Atmos. Environ.* 42 (34), 2008. <https://doi.org/10.1016/j.atmosenv.2008.07.009>.
- Kanakidou, M., Mihalopoulos, N., Kindap, T., Im, U., Vrekoussis, M., Gerasopoulos, E., Dermizaki, E., Unal, A., Kocak, M., Markakis, K., Melas, D., Kouvarakis, G., Youssef, A.F., Richter, A., Hatzianastassiou, N., Hilboll, A., Ebojje, F., von Savigny, C., Ladstaetter-Weissenmayer, A., Burrows, J., Moubasher, H., 2011. Megacities as hot spots of air pollution in the East Mediterranean. *Atmos. Environ.* 1223–1235 [bind 45](https://doi.org/10.1016/j.atmosenv.2011.06.045).
- Kasparoglu, S., Incecik, S., Topcu, S., 2018. Spatial and temporal variation of O₃, NO and NO₂ concentrations at rural and urban sites in Marmara region of Turkey. *Atmos. Pollut. Res.* 9 (6), 1009–1020. <https://doi.org/10.1016/j.apr.2018.03.005>.
- Khoder, M.I., 2009. Diurnal, seasonal and weekdays-weekends variations of ground level ozone concentrations in an urban area in greater Cairo. *Environ. Monit. Assess.* 149 (1–4), 349–362. <https://doi.org/10.1007/s10661-008-0208-7>.
- Kleanthous, Savvas, Vrekoussis, M., Mihalopoulos, N., Kalabokas, P., Lelieveld, J., 2014. On the temporal and spatial variation of ozone in Cyprus. *Sci. Total Environ.* 476–477, 677–687. <https://doi.org/10.1016/j.scitotenv.2013.12.101>.
- Kohonen, T., 1990. The self-organizing map. *Proc. IEEE* 78 (9), 1464–1480. <https://doi.org/10.1109/5.58325>.
- Kopanakis, I., Glytsos, T., Kouvarakis, G., Gerasopoulos, E., Mihalopoulos, N., Lazaridis, M., 2016. Variability of ozone in the eastern Mediterranean during a 7-year study. *Air Qual. Atmos. Health* 9 (5), 461–470. <https://doi.org/10.1007/s11869-015-0362-3>.
- Kouvarakis, G., Vrekoussis, M., Mihalopoulos, N., Kourtidis, K., Rappenglueck, B., Gerasopoulos, E., Zerefos, C., 2002. Spatial and temporal variability of tropospheric ozone (O₃) in the boundary layer above the Aegean Sea (eastern Mediterranean). *J. Geophys. Res. Atmos.* 107 (18). <https://doi.org/10.1029/2000JD000081> PAU 4-1-PAU 4-14.
- Kumari, S., Jayaraman, G., Ghosh, C., 2013. Analysis of long-term ozone trend over Delhi and its meteorological adjustment. *Int. J. Environ. Sci. Technol.* 10 (6), 1325–1336. <https://doi.org/10.1007/s13762-012-0162-3>.
- Ladstätter-Weissenmayer, A., Kanakidou, M., Meyer-Arneke, J., Dermizaki, E.V., Richter, A., Vrekoussis, M., Wittrock, F., Burrows, J.P., 2007. Pollution events over the East Mediterranean: synergistic use of GOME, ground-based and sonde observations and models. *Atmos. Environ.* 41 (34), 7262–7273. <https://doi.org/10.1016/j.atmosenv.2007.05.031>.
- Lamarque, J.-F., Bond, T.C., Eyring, V., Granier, C., Heil, A., Klimont, Z., Lee, D., Liousse, C., Mieville, A., Owen, B., Schultz, M.G., Shindell, D., Smith, S.J., Stehfest, E., Van Aardenne, J., Cooper, O.R., Kainuma, M., Mahowald, N., McConnell, J.R., Naik, K., van Vuuren, D.P., 2010. Historical (1850–2000) gridded anthropogenic and biomass burning emissions of reactive gases and aerosols: methodology and application. *Atmos. Chem. Phys.* 10, 7017–7039. <https://doi.org/10.5194/acp-10-7017-2010>.
- Laughner, J., Cohen, R.C., 2019. Direct observation of changing NO_x lifetime in north american cities. *Science* 366 (6466), 723–727. <https://science.sciencemag.org/content/366/6466/723.full>.
- Lelieveld, J., Berresheim, H., Borrmann, S., Crutzen, P.J., Dentener, F.J., Fischer, H., Feichter, J., Flatau, P.J., Heland, J., Holzinger, R., Korrman, R., Lawrence, M.G., Levin, Z., Markowicz, K.M., Mihalopoulos, N., Minikin, A., Ramanathan, V., De Reus, M., Roelofs, G.J., Scheeren, H.A., Sciare, J., Schlager, H., Schultz, M., Siegmund, P., Steil, B., Stephanou, E.G., Stier, P., Traub, M., Warneke, C., Williams, J., Ziereis, H., 2002. Global air pollution crossroads over the Mediterranean. *Science* 298 (5594), 794–799. <https://doi.org/10.1126/science.1075457>.
- Lelieveld, J., Hoor, P., Jöckel, P., Pozzer, A., Hadjinicolaou, P., Cammas, J.-P., Beirle, S., 2009. Severe ozone air pollution in the Persian Gulf region. *Atmos. Chem. Phys.* 9 (4), 1393–1406. <https://doi.org/10.5194/acp-9-1393-2009>.
- Lelieveld, J., Evans, J.S., Fnais, M., Giannadaki, D., Pozzer, A., 2015. The contribution of outdoor air pollution sources to premature mortality on a global scale. *Nature* 525 (7569), 367–371. <https://doi.org/10.1038/nature15371>.
- Lelieveld, J., Klingmüller, K., Pozzer, A., Pöschl, U., Fnais, M., Daiber, A., Münzel, T., 2019. Cardiovascular disease burden from ambient air pollution in Europe reassessed using novel hazard ratio functions. *Eur. Heart J.* 40 (20), 1590–1596. <https://doi.org/10.1093/eurheartj/ehz135>.
- Liu, F., Beirle, S., Zhang, Q., Dörner, S., He, K., Wagner, T., 2016. NO_x lifetimes and emissions of cities and power plants in polluted background estimated by satellite observations. *Atmos. Chem. Phys.* 16 (8), 5283–5298. <https://doi.org/10.5194/acp-16-5283-2016>.
- Liu, C., Yin, P., Chen, R., Meng, X., Wang, L., Niu, Y., Lin, Z., Liu, Y., Liu, J., Qi, J., You, J., Kan, H., Zhou, M., 2018. Ambient carbon monoxide and cardiovascular mortality: a nationwide time-series analysis in 272 cities in China. *e12-e18 Lancet Planet Health* 2 (1). [https://doi.org/10.1016/S2542-5196\(17\)30181-X](https://doi.org/10.1016/S2542-5196(17)30181-X) Epub 2018 Jan 9. Erratum in: *Lancet Planet Health*. 2018 Jun;2(6):e243. PMID: 29615203.
- Masiol, M., Squizzato, S., Formenton, G., Harrison, R.M., Agostinelli, C., 2017. Air quality across a European hotspot: spatial gradients, seasonality, diurnal cycles and trends in the Veneto region, NE Italy. *Sci. Total Environ.* 576, 210–224. <https://doi.org/10.1016/j.scitotenv.2016.10.042>.
- Mavroidis, I., Iliä, M., 2012. Trends of NO_x, NO₂ and O₃ concentrations at three different types of air quality monitoring stations in Athens, Greece. *Atmos. Environ.* 63 (2), 135–147. <https://doi.org/10.1016/j.atmosenv.2012.09.030>.
- Meng, Z.Y., Xu, X.B., Yan, P., Ding, G.A., Tang, J., Lin, W.L., Xu, X.D., Wang, S.F., 2009. Characteristics of trace gaseous pollutants at a regional background station in northern China. *Atmos. Chem. Phys.* 9 (3), 927–936. <https://doi.org/10.5194/acp-9-927-2009>.
- Minkos, A., Dauert, U., Feigenspan, S., Kessinger, S., Nordmann, S., Himpel, T., 2018. Luftqualität 2017. Umweltbundesamt, p. 28. <https://www.umweltbundesamt.de/publikationen/luftqualitaet-2017>.
- Monks, P.S., Archibald, A.T., Colette, A., Cooper, O., Coyle, M., Derwent, R., Fowler, D., Granier, C., Law, K.S., Mills, G.E., Stevenson, D.S., Tarasova, O., Thouret, V., von Schneidmesser, E., Sommariva, R., Wild, O., Williams, M.L., 2015. Tropospheric ozone and its precursors from the urban to the global scale from air quality to short-lived climate forcer. *Atmos. Chem. Phys.* 15 (15), 8889–8973. <https://doi.org/10.5194/acp-15-8889-2015>.
- Mostafa, A.N., Zakey, A.S., Monem, S.A., Abdel Wahab, M.M., 2018. Analysis of the surface air quality measurements in the greater Cairo (Egypt) metropolis. *Glob. J. Adv. Res.* 22 (6), 207–214. <https://www.researchgate.net/publication/326548302>.
- Mouzourides, P., Kumar, P., Neophytou, M.K.A., 2015. Assessment of long-term measurements of particulate matter and gaseous pollutants in south-East Mediterranean. *Atmos. Environ.* 107 (2), 148–165. <https://doi.org/10.1016/j.atmosenv.2015.02.031>.
- Myhre, G., Aas, W., Cherian, R., Collins, W., Faluvegi, G., Flanner, M., Forster, P., Hodnebrog, Ø., Klimont, Z., Lund, M.T., Mülmenstädt, J., Lund Myhre, C., Olivieri, D., Prather, M., Quaas, J., Samset, B.H., Schnell, J.L., Schulz, M., Shindell, D., Skeie, R.B., Takemura, T., Tsyro, S., 2017. Multi-model simulations of aerosol and ozone radiative forcing due to anthropogenic emission changes during the period 1990–2015. *Atmos. Chem. Phys.* 17, 2709–2720. <https://doi.org/10.5194/acp-17-2709-2017>.
- Ninneman, M., Marto, J., Shaw, S., Edgerton, E., Blanchard, C., Schwab, J., 2021. Reactive oxidized nitrogen speciation and partitioning in urban and rural New York State. *J. Air Waste Manag. Assoc.* 71 (3), 348–365. <https://doi.org/10.1080/109662247.2020.1837289>.
- Notario, A., Bravo, I., Adame, J.A., Díaz-de-Mera, Y., Aranda, A., Rodríguez, A., Rodríguez, D., 2012. Analysis of NO, NO₂, NO_x, O₃ and oxidant (O_x = O₃ + NO₂) levels measured in a metropolitan area in the southwest of Iberian Peninsula. *Atmos. Res.* 104–105 (2), 217–226. <https://doi.org/10.1016/j.atmosres.2011.10.008>.
- Ozdemir, H., Ozdemir, H., Im, U., Kostandinou, M., Agacayak, T., Unal, A., Kindap, T., Khan, M., 2009. Impacts of Istanbul emissions on regional air quality: quantification using model-3 framework and trajectory analysis. Retrieved February 8, 2021, from <http://citeseerx.ist.psu.edu/viewdoc/summary?doi=10.1.1.600.3585>.
- Panayiotou, G.P., Kalogirou, S.A., Florides, G.A., Maxoulis, C.N., Papadopoulos, A.M., Neophytou, M., Georgakis, G., 2010. The characteristics and the energy behaviour of the residential building stock of Cyprus in view of directive 2002/91/EC. *Energy Build.* 42 (4), 2083–2089.

- Parrish, D.D., 2006. Critical Evaluation of US On-road Vehicle Emission Inventories. 40, pp. 2288–2300. <https://doi.org/10.1016/j.atmosenv.2005.11.033>.
- Parrish, D.D., Kuster, W.C., Shao, M., Yokouchi, Y., Kondo, Y., Goldan, P.D., de Gouw, J.A., Koike, M., Shirai, T., 2009. Comparison of air pollutant emissions among mega-cities. *Atmos. Environ.* 43 (40), 6435–6441. <https://doi.org/10.1016/j.atmosenv.2009.06.024>.
- Pikridas, M., Vrekoussis, M., Sciare, J., Kleanthous, S., Vasiliadou, E., Kizas, C., Savvides, C., Mihalopoulos, N., 2018. Spatial and temporal (short and long-term) variability of submicron, fine and sub-10 μm particulate matter (PM_{10} , $\text{PM}_{2.5}$, PM_{10}) in Cyprus. *Atmos. Environ.* 191. <https://doi.org/10.1016/j.atmosenv.2018.07.048>.
- Pisso, I., Sollum, E., Grythe, H., Kris, N.I., Cassiani, M., Eckhardt, S., Arnold, D., Morton, D., Thompson, R.L., Groot, C.D., Evangelio, N., Sodemann, H., Haimberger, L., Brunner, D., Burkhardt, J.F., Fouilloux, A., Brioude, J., 2019. *The Lagrangian Particle Dispersion Model Introduction: FLEXPART History and Recent Updates*.
- Pope III, C.A., 2002. Lung cancer, cardiopulmonary mortality, and long-term exposure to fine particulate air pollution. *JAMA* 287 (9), 1132. <https://doi.org/10.1001/jama.287.9.1132>.
- Pusede, S.E., Gentner, D.R., Wooldridge, P.J., Browne, E.C., Rollins, A.W., Min, K.E., Russell, A.R., Thomas, J., Zhang, L., Brune, W.H., Henry, S.B., Digangi, J.P., Keutsch, F.N., Harrold, S.A., Thornton, J.A., Beaver, M.R., St. Clair, J.M., Wennberg, P.O., Sanders, J., Cohen, R.C., 2014. On the temperature dependence of organic reactivity, nitrogen oxides, ozone production, and the impact of emission controls in San Joaquin Valley, California. *Atmos. Chem. Phys.* 14 (7), 3373–3395. <https://doi.org/10.5194/acp-14-3373-2014>.
- Querol, X., Alastuey, A., Pandolfi, M., Reche, C., Pérez, N., Minguillón, M.C., Moreno, T., Viana, M., Escudero, M., Orto, A., Pallarés, M., Reina, F., 2014. 2001–2012 trends on air quality in Spain. *Sci. Total Environ.* 490, 957–969. <https://doi.org/10.1016/j.scitotenv.2014.05.074>.
- Rauthe-Schöch, A., Baker, A.K., Schuck, T.J., Brennkneijer, C.A.M., Zahn, A., Hermann, M., Stratmann, G., Ziereis, H., Van Velthoven, P.F.J., Lelieveld, J., 2016. Trapping, chemistry, and export of trace gases in the south asian summer monsoon observed during CARIBIC flights in 2008. *Atmos. Chem. Phys.* 16 (5), 3609–3629. <https://doi.org/10.5194/acp-16-3609-2016>.
- Rumelhart, D.E., Zipser, D., 1986. Feature discovery by competitive learning. In: Rumelhart, D.E., Hinton, G.E., Williams, R.J. (Eds.), *Parallel Distributed Processing*. Vol. 1. MIT Press, Cambridge MA, pp. 151–193.
- Scheeren, H.A., Lelieveld, J., Roelofs, G.J., Williams, J., Fischer, H., De Reus, M., De Gouw, J.A., Warneke, C., Holzinger, R., Schlager, H., Klüpfel, T., Bolder, M., Van Der Veen, C., Lawrence, M., 2003. The impact of monsoon outflow from India and Southeast Asia in the upper troposphere over the eastern Mediterranean. *Atmos. Chem. Phys.* 3 (5), 1589–1608. <https://doi.org/10.5194/acp-3-1589-2003>.
- Schindlbacher, A., Zechmeister-Boltenstern, S., Butterbach-Bahl, K., 2004. Effects of soil moisture and temperature on NO , NO_2 , and N_2O emissions from European forest soils. *J. Geophys. Res.* D: Atmos. 109 (17), 1–12. <https://doi.org/10.1029/2004JD004590>.
- Seibert, P., Frank, A., 2004. Source-receptor matrix calculation with a lagrangian particle dispersion model in backward mode. *Atmos. Chem. Phys.* 4, 51–63. <https://doi.org/10.5194/acp-4-51-2004>.
- Seinfeld, J.H., Pandis, S.N., 2006. *Atmospheric Chemistry and Physics: From Air Pollution to Climate Change*. 2nd edition. John Wiley & Sons, New York.
- Selden, T.M., Song, D., 1994. Environmental quality and development: is there a kuznets curve for air pollution Emissions? *J. Environ. Econ. Manag.* 27 (2), 147–162. <https://doi.org/10.1006/jeem.1994.1031>.
- Serça, D., Delmas, R., Le Roux, X., Parsons, D.A.B., Scholes, M.C., Abbadi, L., Lensi, R., Ronce, O., Labroue, L., 1998. Comparison of nitrogen monoxide emissions from several african tropical ecosystems and influence of season and fire. *Glob. Biogeochem. Cycles* 12 (4), 637–651. <https://doi.org/10.1029/98GB02737>.
- Shen, L., Mickley, L.J., Gilleland, E., 2016. Impact of increasing heat waves on U.S. Ozone episodes in the 2050s: results from a multimodel analysis using extreme value theory. *Geophys. Res. Lett.* 43 (8), 4017–4025. <https://doi.org/10.1002/2016GL068432>.
- Sillman, S., He, D., 2002. Some theoretical results concerning O_3 - NO_x -VOC chemistry and NO_x -VOC indicators. *J. Geophys. Res. Atmos.* 107 (22). <https://doi.org/10.1029/2001JD001123> ACH 26–1.
- Singh, H.B., 2015. Tropospheric chemistry and composition: peroxyacetyl nitrate. *Encyclopedia of Atmospheric Sciences*, Second edition Elsevier Inc., pp. 251–254 <https://doi.org/10.1016/B978-0-12-382225-3.00433-3>.
- Singh, K.P., Bartolucci, A.A., Bae, S., 2001. Mathematical modeling of environmental data. *Math. Comput. Model.* 33, 793–800.
- Steiner, A.L., Davis, A.J., Sillman, S., Owen, R.C., Michalak, A.M., Fiore, A.M., 2010. Observed suppression of ozone formation at extremely high temperatures due to chemical and biophysical feedbacks. *Proc. Natl. Acad. Sci.* 107 (46), 19685–19690. <https://doi.org/10.1073/pnas.1008336107>.
- Steiner, A.L., Tawfik, A.B., Shalaby, A., Zakey, A.S., Abdel-Wahab, M.M., Salah, Z., Solmon, F., Sillman, S., Zaveri, R.A., 2014. Climatological simulations of ozone and atmospheric aerosols in the greater Cairo region. *Clim. Res.* 59 (3), 207–228. <https://doi.org/10.3354/cr012111>.
- Trainer, M., 1993. Correlation of ozone with NO_y in photochemically aged air. *J. Geophys. Res.* 98 (D2), 2917–2925. <https://doi.org/10.1029/92JD01910>.
- Veefkind, J.P., Aben, I., McMullan, K., Förster, H., de Vries, J., Otter, G., Claas, J., Eskes, H.J., de Haan, J.F., Kleipool, Q., van Weele, M., Hasekamp, O., Hoogeveen, R., Landgraf, J., Snel, R., Tol, P., Ingmann, P., Voors, R., Kruijzinga, B., Vink, R., Visser, H., Levelt, P.F., 2012. TROPOMI on the ESA Sentinel-5 precursor: a GMES mission for global observations of the atmospheric composition for climate, air quality and ozone layer applications. *Remote Sens. Environ.* 120, 70–83. <https://doi.org/10.1016/j.rse.2011.09.027>.
- Viana, M., Hammings, P., Colette, A., Querol, X., Degraeuwe, B., de Vlieger, I., van Aardenne, J., 2014. Impact of maritime transport emissions on coastal air quality in Europe. *Atmospheric Environment* Vol. 90. Elsevier Ltd., pp. 96–105. <https://doi.org/10.1016/j.atmosenv.2014.03.046>.
- Volz, A., Kley, D., 1988. Evaluation of the montsouris series of ozone measurements made in the nineteenth century. *Nature* 332 (6161), 240–242. <https://doi.org/10.1038/332240a0>.
- Von Glasow, R., 2008. Atmospheric chemistry: pollution meets sea salt. *Nature Geoscience*. Vol. 1. Nature Publishing Group, pp. 292–293. <https://doi.org/10.1038/ngeo192> Issue 5.
- von Glasow, R., Bobrowski, N., Kern, C., 2009. The effects of volcanic eruptions on atmospheric chemistry. *Chem. Geol.* 263 (1–4), 131–142. <https://doi.org/10.1016/j.chemgeo.2008.08.020>.
- Vrekoussis, M., Richter, A., Hilboll, A., Burrows, J.P., Gerasopoulos, E., Lelieveld, J., Barrie, L., Zerefos, C., Mihalopoulos, N., 2013. Economic crisis detected from space: air quality observations over Athens/Greece. *Geophys. Res. Lett.* 40 (2). <https://doi.org/10.1002/grl.50118>.
- Wang, S.X., Zhao, B., Cai, S.Y., Klimont, Z., Nielsen, C., McElroy, M.B., Morikawa, T., Woo, J.H., Kim, Y., Fu, X., Xu, J.Y., Hao, J.M., He, K.B., 2014. Emission trends and mitigation options for air pollutants in East Asia. *Atmos. Chem. Phys. Discuss.* 14 (2), 2601–2674. <https://doi.org/10.5194/acpd-14-2601-2014>.
- Wang, X., Jacob, D.J., Eastham, S.D., Sulprizio, M.P., Zhu, L., Chen, Q., Alexander, B., Sherwen, T., Evans, M.J., Lee, B.H., Haskins, J.D., Lopez-Hilfiker, F.D., Thornton, J.A., Huey, G.L., Liao, H., 2019. The role of chlorine in global tropospheric chemistry. *Atmos. Chem. Phys.* 19, 3981–4003. <https://doi.org/10.5194/acp-19-3981-2019>.
- Weaver, C.P., Liang, X.Z., Zhu, J., Adams, P.J., Amar, P., Avise, J., Caughey, M., Chen, J., Cohen, R.C., Cooter, E., Dawson, J.P., Gilliam, R., Gilliland, A., Goldstein, A.H., Gramsch, A., Grano, D., Guenther, A., Gustafson, W.I., Harley, R.A., Wuebbles, D.J., 2009. A preliminary synthesis of modeled climate change impacts on U.S. Regional ozone concentrations. *Bull. Am. Meteorol. Soc.* 90 (12), 1843–1863. <https://doi.org/10.1175/2009BAMS2568.1>.
- WHO, 2005. https://www.euro.who.int/_data/assets/pdf_file/0008/147851/E87950.pdf.
- Winkler, S.L., Anderson, J.E., Garza, L., Ruona, W.C., Vogt, R., Wallington, T.J., 2018. Vehicle criteria pollutant (PM, NO_x , CO, HCs) emissions: how low should we go? *Npj Clim. Atmos. Sci.* 1 (1). <https://doi.org/10.1038/s41612-018-0037-5>.
- Yienger, J.J., Levy, I.I., 1995. Empirical model of global soil-biogenic NO_x emissions. *J. Geophys. Res.* 100 (x).
- Zellweger, C., Forrer, J., Hofer, P., Nyeki, S., Schwarzenbach, B., Weingartner, E., Ammann, M., Baltensperger, U., Baltensperger, U., 2003. Partitioning of reactive nitrogen (NO_y) and dependence on meteorological conditions in the lower free troposphere Atmospheric Chemistry and Physics Partitioning of reactive nitrogen (NO_y) and dependence on meteorological conditions in the lower free troposphere. Issue 3 European Geosciences Union. Vol. 3. www.atmos-chem-phys.org/acp/3/779/.
- Zittis, G., Hadjinicolaou, P., Fnaiss, M., Lelieveld, J., 2016. Projected changes in heat wave characteristics in the eastern Mediterranean and the Middle East. *Reg. Environ. Chang.* 16 (7), 1863–1876. <https://doi.org/10.1007/s10113-014-0753-2>.